STRESS CORROSION CRACKING OF ALLOY 152 WELD BUTTER NEAR THE LOW ALLOY STEEL INTERFACE

Bogdan Alexandreanu, Yiren Chen, Ken Natesan, and Bill Shack

Argonne National Laboratory, Nuclear Engineering Division,

9700 S. Cass Avenue, Argonne IL 60439, USA

ABSTRACT

The objective of this work was to obtain SCC growth data in Alloy 152 weld butter near the interface with Low Alloy Steel (LAS), which is a region where some dilution of Cr was expected to have occurred, thus presumably exhibiting an increased SCC-susceptibility vs. the bulk of the weld. The LAS piece used in this application was Alloy 533-Gr B from the Midland reactor lower head, and the Alloy 152 weld butter received a prototypical Post Weld Heat Treatment (PWHT) prior to joining by Alloy 152 to an Alloy 690 piece according to a procedure qualified to ASME Section IX. The compact tension specimens for SCC testing were aligned in the first layer of the Alloy 152 butter. The experimental approach based on tracking environmental enhancement vs. location was successful in identifying SCC-susceptible locations, and SCC rates ranging from 10^{-12} m/s to as high as 10^{-10} m/s were measured. The post-test examination of the specimens found that the fracture had the intergranular/interdendritic appearance typical of welds, and that the propagation was arrested wherever an intersection with the LAS occurred. The large range of SCC rates measured does not appear to correlate well with the local concentration of Cr (approx. 25% at the SCC locations), and, in fact, low Cr (20%) – high Fe "streaks" seemed to slow/arrest crack propagation. In short, simple "Cr dilution" does not seem to fully account for the "SCC-susceptible" microstructure that yielded the 10^{-10} m/s growth rate in this weld.

Keywords: Stress Corrosion Cracking, Alloy 152, Cr dilution

1. INTRODUCTION

Nickel-base Alloy 600 was used as construction material in light water reactors (LWRs), and has over the years been prone to stress corrosion cracking (SCC). Such cracking was first observed in steam generator tubes, but it has also occurred in components such as instrument nozzles and heater thermal sleeves in the pressurizer and control-rod drive mechanism (CRDM) housings in reactor vessel closure heads. In operating plants, weld Alloys 82 and 182 have been used with Alloy 600. Alloy 690 is currently the replacement material of choice for Alloy 600 due to its higher Cr content. This choice was made following numerous laboratory studies worldwide which established an excellent resistance to stress corrosion cracking in reactor coolant primary water for this alloy.[1-3] As such, during the last twenty years, thin-walled steam generator tubing for pressurized water reactors (PWRs) has been fabricated from the higher-chromium material, Alloy 690. A few years later, this material has also begun to be used for thick-section components, particularly nozzle penetrations, during the replacement of heads for reactor pressure vessels. This increased use of Alloy 690 has necessitated the use of the weld Alloys 52 and 152, which also have high chromium content.

Despite the increased resistance to SCC of the higher Cr alloy welds in laboratory tests, concern remains for the behavior at the interfaces of dissimilar metal welds (DMWs) where the Cr levels can be diluted. Of special concern are the interfaces with steel where the Cr gradient is the largest. In addition, many PWRs still have DMWs made with the SCC-susceptible Alloy 182/82 at low alloy steel (LAS) vessel nozzle-to-piping DMWs. For these plants where the Alloy 182/82 welds still exist, several mitigation technologies have been applied including structural weld overlays (WOLs) or inlay/onlay welds with higher Cr content weld metals. However, while the higher Cr welds exhibit an improved SCC resistance in laboratory tests, the behavior at the LAS interface where dilution of Cr occurs is less well understood.

Recently-completed SCC crack growth testing conducted at Argonne National Laboratory (ANL) on an Alloy 52M WOL showed that SCC behavior at DMW interfaces is indeed of concern.[4,5] As such, testing of an Alloy 52M (30 wt. % Cr) WOL deposited with prototypical welding parameters on an existing Alloy 182 weld (15 wt. % Cr) found that the SCC crack growth rate (CGR) increased substantially in the Cr-diluted regions near the interface with Alloy 182. The diluted area (24.5 wt. % Cr) of Alloy 52M had an SCC CGR only two times lower than that the MRP-115 75th percentile curve for Alloy 182[6], and the interface between the two welds behaved just like predicted by the MRP-115 75th percentile curve for Alloy 182.[6] One of the most interesting features observed on the fracture surface of the two Cr-diluted welds, 52M WOL and 152-LAS, is that cracking occurred in a direction normal to the weld dendritic grains – a direction which is not typically associated with fast SCC CGRs in welds. In summary, limited testing and microstructural analysis to date seem to indicate that the benefits of the SCC-resistant weld material appear uncertain in the regions at or near the interface, and one of the major culprits seems to be the dilution of Cr near the interface.

The objective of the work presented in this paper was to obtain SCC CGR data in the first layer of an Alloy 152 butter deposited on LAS. For this purpose, CGR test specimens were aligned in the region of interest, and the experimental approach was based on a closely monitoring the environmental enhancement of the cyclic response. The Cr levels were determined along the actual SCC path during the post-test examination of the specimens.

2. EXPERIMENT

This section describes the weld fabrication, test specimens, and the CGR test apparatus and experimental approach.

2.1 Alloy 690 to Alloy 522 grade B joint

The following subsection documents the steps taken to produce a 3-inch thick butt weld for Alloy 690 (Heat NX3297HK12) welded to SA-533 Gr B class 1 Steel (Heat A5401 from the Midland reactor lower head) buttered with Alloy 152 filler metal. The geometry of the joint is shown in Fig. 1. The joint was designed with a straight edge on the Alloy 690 side to facilitate SCC CGR testing of the Alloy 690 HAZ. The welding procedure was qualified to ASME Section IX by ANL Central Shops.

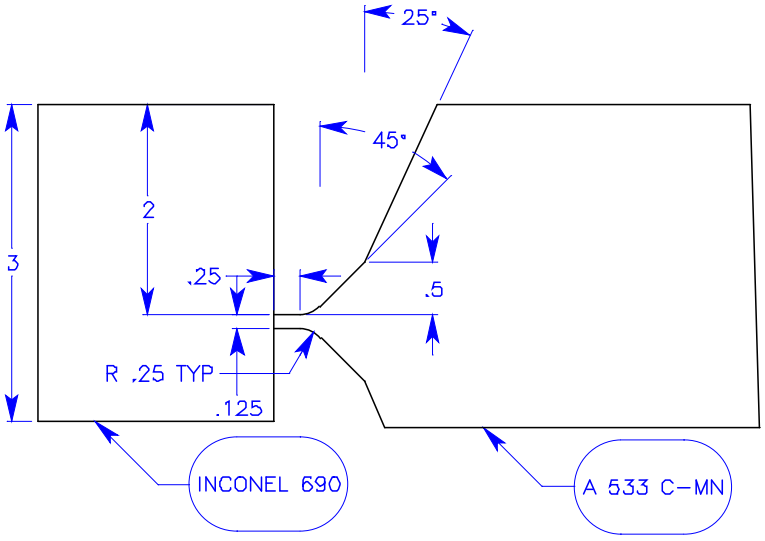

Figure 1. Joint design, Alloy 690 to SA-533 Gr B. Units are in inch.

2.1.1 Alloy 152 Weld Buttering

The LAS plate was machined with a bevel on one end. The beveled end was buttered with Alloy 152 F43 filler metal per a Welding Procedure Specification (WPS) developed and qualified by ANL. A record was kept of the number and location of weld passes together with the heat code of the filler metal used, and the welding parameters that were used. This record is shown in Table 1.

Table 1. Welding process and conditions for various weld passes used for fabricating the A152 butter.

Weld Pass	Process	Filler Metal	Filler Size, in.	Heat Code	Type Polarity	Current, A	Voltage, V	Travel Speed, in./min	Notes
1 - 23	SMAW	Alloy 152, ENiCrFe-7	1/8	720129	DCRP	97-102	21 - 23	5	Layer 1 LP
24-44	SMAW	Alloy 152, ENiCrFe-7	5/32	146444	DCRP	113-117	25 - 26	5	Layer 2 LP
45-65	SMAW	Alloy 152, ENiCrFe-7	5/32	146444	DCRP	113-117	25 - 26	5	Layer 3 LP

After each layer, a liquid penetrant (LP) check was performed. After buttering, the LAS piece was stress relieved at 1150 ± 25ºF for 3h.

2.1.2 Alloy 152 Butt Weld

The buttered LAS piece described in the previous sub-section was beveled on the buttered edge leaving ¼" of F43 weld material on the face, and a section of Alloy 690 plate was used to make the opposing part of the butt weld. A double bevel J grove weld was produced using a WPS developed and qualified by ANL. The joint design appears as shown in Fig. 3, and the number and location of weld passes together with the heat code of the filler metal used, as well as the welding parameters are given in Table 2.

Table 2. Welding process and conditions for various weld passes used for fabricating the A152 butt weld.

Weld Pass	Process	Filler Metal	Filler Size, in.	Heat Code	Type Polarity	Current, A	Voltage, V	Travel Speed, in./min	Notes
1 - 8	SMAW	Alloy 152, ENiCrFe-7	1/8	720129	DCRP	97-102	21 - 23	5	
9-14	SMAW	Alloy 152, ENiCrFe-7	1/8	146444	DCRP	97-102	25 - 26	5	Root LP BG LP
15-26	SMAW	Alloy 152, ENiCrFe-7	5/32	146444	DCRP	113-117	25 - 26	5	Final LP
27-76	SMAW	Alloy 152, ENiCrFe-7	1/8	WCO4F6	DCRP	97-102	25 - 26	5	Final LP

The root pass of the weld and back grind was LP tested, and the final weld surface was also LP tested. The final weld was radiographed per ASME Section IX.

2.2 SCC CGR testing

The SCC CGR testing conducted in test facilities equipped with SS autoclaves configured for CT specimens. A detailed description of these facilities is provided elsewhere.[7-8] Crack extensions were determined by the reversing DC-potential-drop technique. The simulated PWR feed water contained 2 ppm Li, 1000 ppm B, ≈2 ppm dissolved hydrogen (≈23 cm^3/kg), and less than 10 ppb dissolved oxygen (DO). The water was recirculated through the autoclave at a rate 50 ml/min. The test temperature was 320°C.

The CGR tests were conducted using the standard ANL testing approach in which all stages of the test – fatigue precracking, transitioning to SCC, and SCC CGR determinations - are conducted in the primary water environment. Also, in the ANL approach, the cyclic response informs the management of the test. For the specific case of tests on 1st layer welded specimens where the dendritic grains are normal to the test plane, intergranular SCC is likely to be off-plane, in an orientation that prevents the CGR from being

measured by DC potential correctly. Hence, in the current tests, the crack was advanced until an environmental enhancement of similar to that obtained in tests on Alloy 152 in which the direction of propagation was parallel to the dendritic grains. Of reference are tests conducted at ANL on an Alloy 152 weld that was produced in a symmetric, double-J geometry, Fig. 2.[9] In those tests it was found that environmental enhancement peaks during cyclic with load ratios of R = 0.5, and rise time of 600s, and the resulting fracture mode is IG. Based on that experience, a similar level of environmental enhancement in the current tests will be interpreted as IG SCC propagation in a forward direction that can readily be measured by DC potential, and the specimen will be set at constant load.

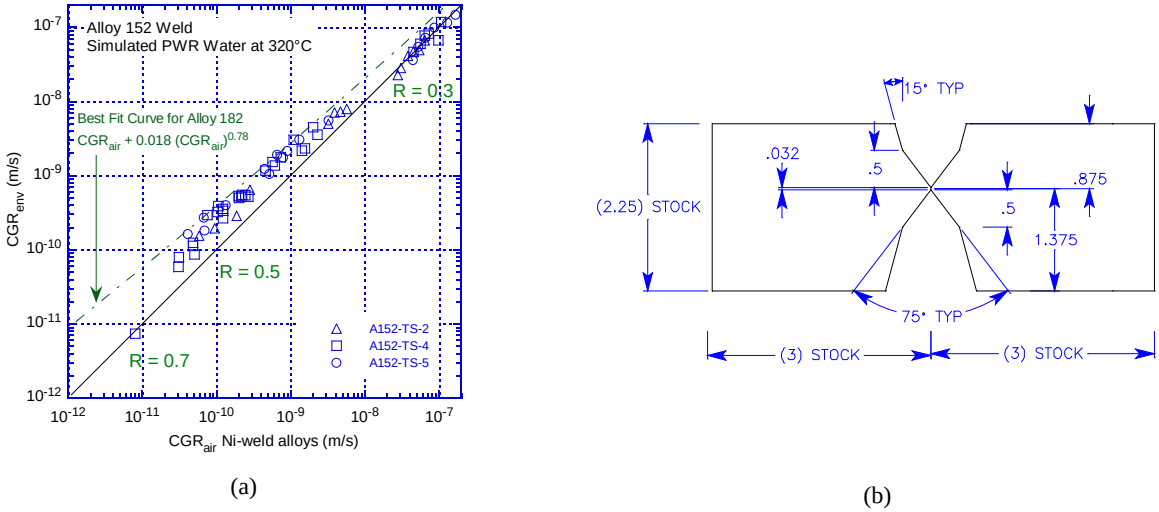

(a) (b)

Figure 2. (a) Cyclic CGR data for the Alloy 152 weld tested in primary water environment, and (b) Alloy 152 weld produced in a double-J geometry.

3. RESULTS

Two tests were completed on Alloy 152 in a 1st layer configuration, and the results will be presented in this section. There was no microstructural characterization conducted prior to machining the specimens. The only requirement for the specimens – produced at ANL Central Shops - was that they be aligned in the 1st weld layer, hence, the specimens sampled random locations in that first layer. The microstructural characterization (with a special attention to Cr concentration) was conducted post-test, along the actual crack path.

3.1 SCC CGR test on 1st Layer Alloy 152 weld butter Specimen N152-LAS-1

Specimen N152-LAS-1 was a 1T CT specimen aligned along the 1st layer of the Alloy 152 butter. Figure 3 shows both sides of that specimen prior to the SCC CGR test. Pictures taken before and after machining the notch have been overlapped to show alignment. The alignment was aimed at the outer region of the Alloy 152, as close to the LAS as was possible achievable. Both sides of this specimen seem to indicate that two lobes of the butter weld are ahead of the crack tip.

The testing conditions for specimen N152-LAS-1 are given in Table 3. The crack was advanced approx. 1.65 mm in fatigue, slightly into the first weld lobe, and transitioning steps were undertaken. The SCC CGR component was first calculated by superposition in test period 4 to be approx. 1.9×10^{-11} m/s, and this rate suggested that the fracture mode was IG. However, it became clear rather quickly that the preferred crack path is off-plane, hence a correct SCC CGR will be difficult to measure by DC potential. To illustrate this point, a visual representation of the test in the framework described previously is shown in Fig. 4. The plots tracks the environmental enhancement of two loading conditions – rise 50s and rise 600s, R = 0.5 – vs. crack advance from the notch. The purpose of the fast cycle is to advance the crack, and the purpose of the slow cycle is to probe for environmental enhancement. The dotted red and blue

horizontal lines represent the enhancement levels of a forward advancing crack based on the Alloy 152 experience (Fig. 2). The large scatter observed in the cyclic response was judged to be indicative of primarily off-plane crack propagation. Overall, Fig. 4 also provides the SCC CGRs and shows that such measurements were attempted mainly at two locations in the specimen where the "conditions" were judged to be optimal from an experimental standpoint.

Select crack length and K_{max} vs. time are shown in Fig. 5 with the purpose of highlighting some of the challenges posed by off-plane cracking. The specimen was set at constant load in period 18 (Fig. 5a) after an increased environmental enhancement had been observed in test periods 14 and 16. Moreover, the SCC CGR component calculated by superposition in test period 17 was in the 10^{-10} m/s range, the highest such determination so far in this test. The resulting SCC CGR was approx. $1.8x10^{-11}$ m/s for the first 1000h, then diminished to approx. $7x10^{-13}$ m/s. At that stage, cycling was reintroduced in test period 19, and it is interesting to note that under cyclic loading the initial measured CGR of $1.2x10^{-9}$ m/s decreases by a factor 5 by the end of the test period (Fig. 5b), suggesting that the ligaments that that had formed during the constant load test period were being broken. If the rate of growth in test period 18 is assumed to have been $1.8x10^{-11}$ m/s for the entire test period, the subsequent (remaining) growth in test period 19 still displays a pronounced curvature (Fig. 5b), and this shape is atypical of corrosion fatigue growth. Hence, a more conservative approach would have been to assume that growth in test period 18 ended where the CGR in test period 19 stabilizes and reaches the expected value of $2.4x10^{-10}$ m/s, making it consistent with test period 16. In this latter case, the conservative SCC CGR for test period 18 is estimated to be $3.7x10^{-11}$ m/s.

An additional example of SCC growth determination is shown in Fig. 5c. As the measured SCC CGR under constant load conditions in the preceding test period 21 was very small, periodic unloading (8h hold, $CGR_{air} \approx 1x10^{-12}$ m/s) was introduced in test period 22 to investigate whether unbroken ligaments are present or not. The SCC CGR measured initially (first 1,000h) in test period 22 was approx. $9.9x10^{-12}$ m/s, then the growth appeared to stop. In order to re-activate the growth, a somewhat more aggressive loading (2h hold, $CGR_{air} \approx 5x10^{-12}$ m/s) was introduced in test period 23 and the response was similar to that observed at the beginning of test period 22. The fact that a similar rate was measured under two different hold times (8h in period 22, and 2h in period 23) suggests that fatigue is not the dominating driving force for crack growth in this specimen. After another "no growth" measurement under constant load conditions in test period (24), the test in water ended, and that was followed by a final fatigue test period in room temperature air.

It is important to note that while the above seemingly "benign" SCC CGR determinations were made by DC potential, massive SCC was taking place off-plane, in a direction almost normal to the test plane.

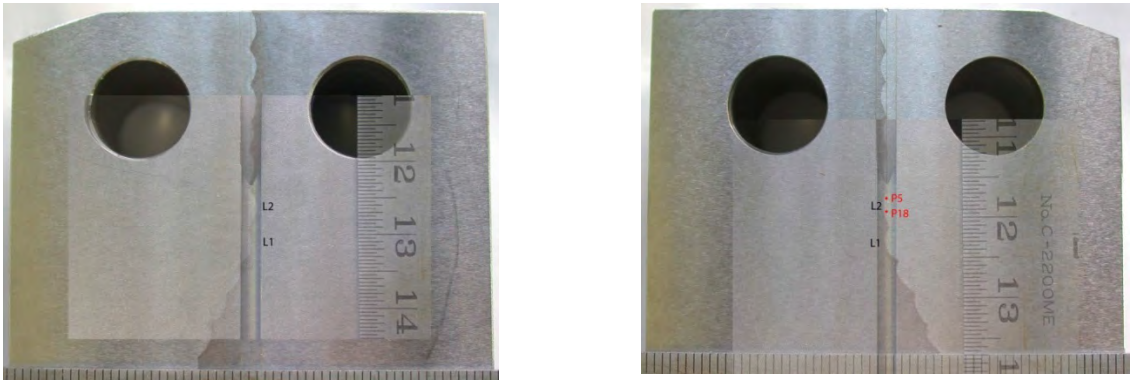

(a) (b)

Figure 3. Specimen N152-LAS-1, overlapped images before and after the specimen notch was machined: (a) side 1, and (b) side 2.

Table 3. Crack growth data for dilution specimen N152-LAS-1 in PWR water[a].

Test Period	Test Time, h	Temp. °C	Load Ratio R	Rise Time, s	Down Time, s	Hold Time, s	K_{max}, MPa·m$^{1/2}$	ΔK, MPa·m$^{1/2}$	CGR_{env}, m/s	Estimated CGR_{air}, m/s	Crack Length, mm
Pre a	145	321.3	0.2	0.5	0.5		21.7	17.4	4.48E-08	1.02E-07	10.480
Pre b	160	321.2	0.2	50	50		21.8	17.4	1.06E-09	1.02E-09	10.515
Pre c	169	321.1	0.2	0.5	0.5		23.1	18.5	9.06E-08	1.30E-07	11.430
Pre d	184	321.2	0.2	50	50		23.3	18.6	1.15E-09	1.34E-09	11.534
Pre e	189	321.1	0.2	0.5	0.5		24.3	19.4	9.01E-08	1.59E-07	12.196
Pre f	193	321.1	0.2	1	1		24.7	19.7	3.60E-08	8.48E-08	12.466
Pre g	208	321.2	0.2	50	50		24.7	19.8	2.26E-09	1.72E-09	12.506
Pre h	214	321.3	0.2	1	1		25.3	20.3	3.56E-08	9.50E-08	12.885
1	234	321.2	0.5	50	12		25.4	12.7	1.12E-09	6.04E-10	12.966
2	305	321.7	0.5	300	12		25.5	12.8	2.66E-10	1.03E-10	13.039
3	575	320.0	0.5	600	12		25.8	12.9	1.32E-10	5.25E-11	13.133
4	976	320.4	0.5	600	12	7,200	25.8	12.9	4.16E-11	4.09E-12	13.171
5	1,742	320.3	1.0	0	0		25.8	0.0	1.99E-11	-	13.201
6	2,421	319.4	0.5	12	12	7,200	26.0	13.0	1.98E-11	4.47E-12	13.262
7	2,680	320.5	1.0	0	0		26.0	0.0	1.47E-11	-	13.279
8	2,917	320.9	0.49	600	12		25.9	13.2	7.49E-11	5.72E-11	13.358
9	3,024	321.1	0.49	50	12		26.1	13.3	6.36E-10	7.07E-10	13.541
10	3,454	320.9	0.49	600	12		26.2	13.4	4.57E-11	6.01E-11	13.628
11	3,862	320.5	0.49	50	12		27.8	14.2	8.37E-10	9.04E-10	14.530
12	3,934	320.1	0.49	600	12		27.8	14.2	1.17E-10	7.54E-11	14.545
13	4,151	320.0	0.49	50	12		29.3	14.9	1.49E-09	1.12E-09	15.366
14	4,294	320.1	0.49	600	12		29.5	15.0	2.13E-10	9.55E-11	15.474
15	4,318	320.0	0.49	50	12		29.6	15.1	1.53E-09	1.18E-09	15.565
16	4,367	320.0	0.49	600	12		29.8	15.2	2.48E-10	9.95E-11	15.605
17	4,534	320.0	0.49	600	12	7,200	29.9	15.3	1.12E-10	7.82E-12	15.693
18	6,879	319.6	1.0	0	0		30.1	0.0	1.82E-11	-	15.839
19	7,026	319.1	0.49	600	12		30.3	15.5	2.48E-10	1.06E-10	16.034
20	7,237	319.5	0.49	600	12	7,200	30.2	15.4	5.46E-11	8.12E-12	16.073
21	7,977	318.7	1.00	0			30.2	0.0	no growth	-	16.073
22	9,701	318.8	0.49	12	12	28,800	30.6	15.6	9.90E-12	2.29E-12	16.115
23	11,411	318.7	0.49	12	12	7,200	30.7	15.6	1.44E-11	9.25E-12	16.211
24	13,060	318.3	1.0	0	0		30.7	0.0	no growth	-	16.211
25	13,068	27.3	0.2	1	1		32.3	25.8	2.80E-08	7.88E-08	16.961

[a]Simulated PWR water with 2 ppm Li, 1000 ppm B, and 2 ppm. DO<10 ppb. Conductivity was 21±3 µS/cm, and pH 6.4.

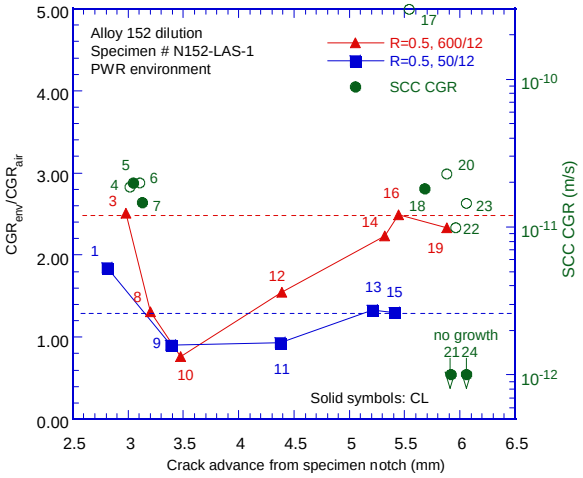

Figure 4. Environmental enhancement of two control test conditions and SCC CGRs vs. distance from the specimen notch for Specimen N152-LAS-1. Test periods are indicated in the figure.

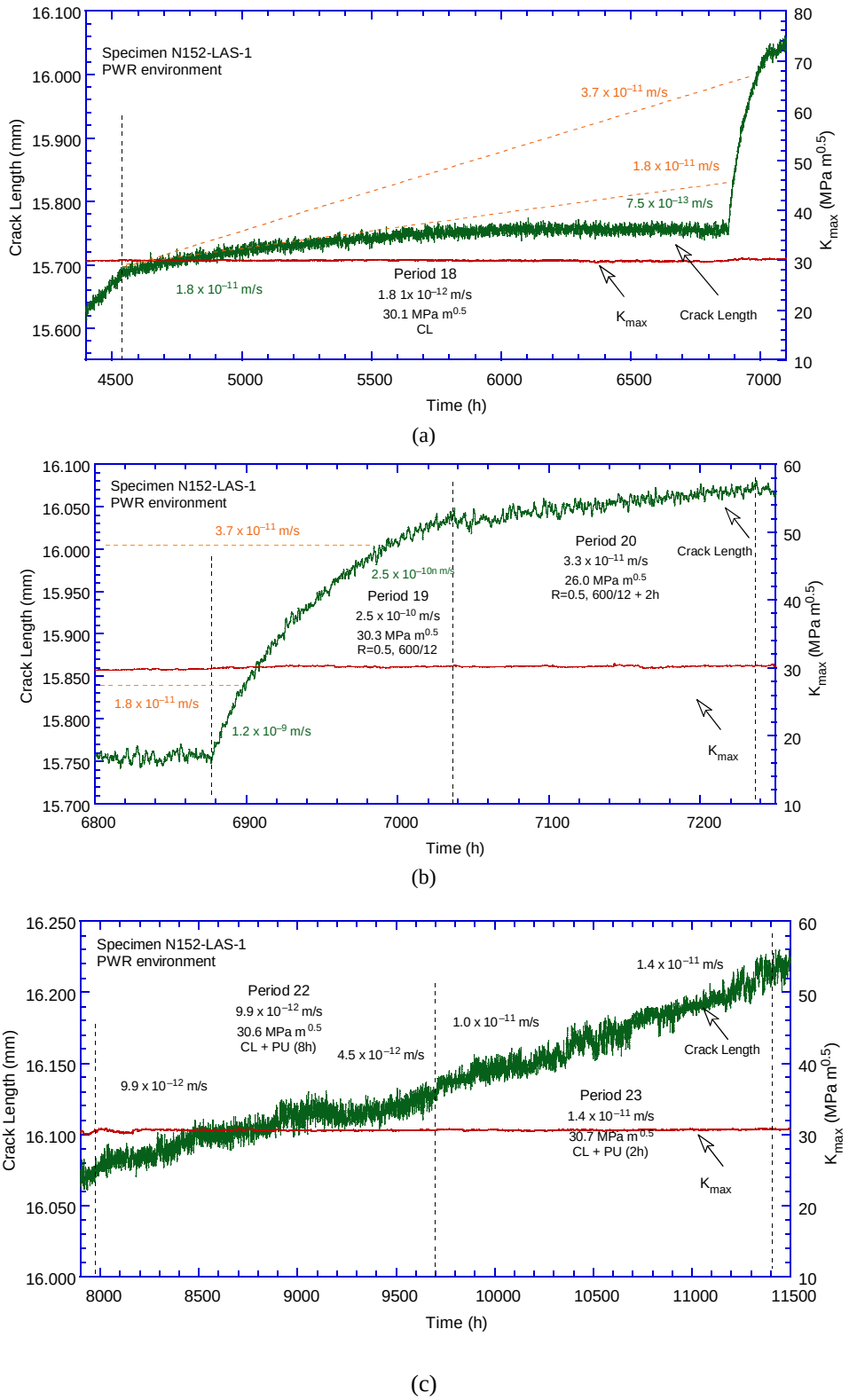

Figure 5. Crack–length–vs.–time for dilution specimen N152-LAS-1 in simulated PWR environment during test periods (a) 18, (b) 19-20, and (c) 22-23.

The post-test examination of specimen N152-LAS-1 involved the examination of both the side surfaces and that of the fracture surface.

For the examination of the side surfaces, the side-grooved sections of the specimens were removed by wire cutting, and the resulting flat surfaces were polished and etched electrochemically in a 10% nital solution. Following this exposure, the resulting weld surface was still shiny while the LAS surface became dull. Nevertheless, the outcome (Fig. 6) shows that the test went largely as planned (see for comparison Fig. 3).

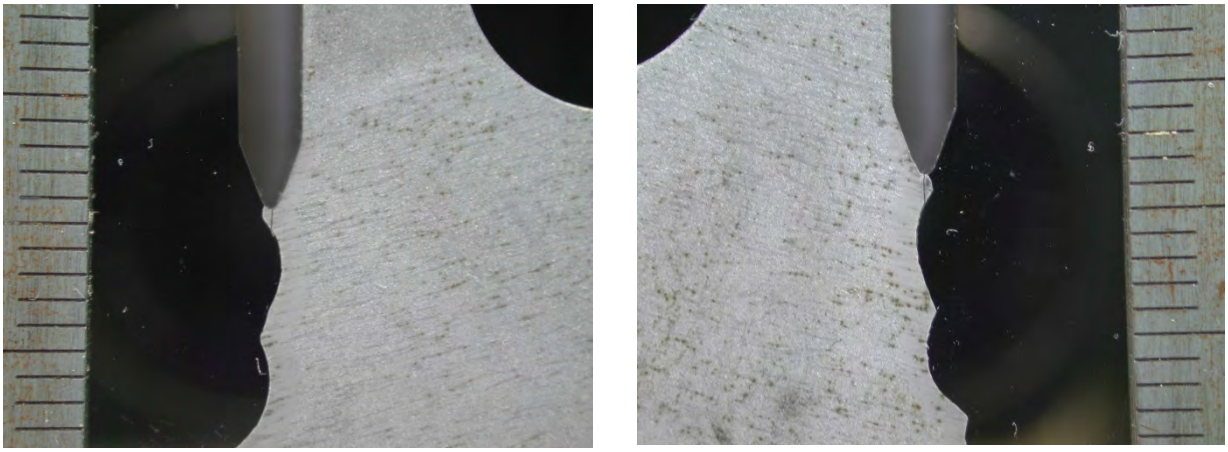

(a) (b)

Figure 6. The two sides of the dilution specimen N152-LAS-1 after testing in primary water.

Figures 7 and 8 are SEM images of the two cross sections. Areas of interest are shown at higher magnification in each figure. As described previously, the crack started from the notch in the LAS, then, upon reaching the Alloy 152 interface, it continued along the interface. Eventually, in both cases, the crack made its way into the weld. The crack hit the LAS interface once more towards the end of the test. This location is marked LAS-i in Fig. 7.

Figures 7 is the best illustration of the evolution of this test. After advancing in the LAS and along the LAS-Alloy 152 interface in fatigue, the crack turned into the weld, and the first attempts at an SCC CGR measurement were made at location 1, Fig. 7a. The crack appears to follow the direction of the interdendritic grains rather than that of the test plane. The first set of chemical composition measurements were conducted at this location by SEM Energy Dispersive X-ray (EDX) and yielded an average 27 Cr - 21.4 Fe – 51.5 Ni (Fig. 7b). Next, the crack advanced into the weld, intersected the LAS interface one more time (location marked LAS-i), then turned decisively into the weld, and propagated along the direction of the dendritic grains, normal to the original crack direction, Fig. 7c. Chemical composition measurements were conducted in this region and yielded an average 24.1 Cr - 31.4 Fe – 43.5 Ni (Fig. 7c).

Figure 8 is largely similar to Fig. 7. The higher magnification micrographs capture the location where the crack left the LAS-Alloy 152 interface and started propagating into the Alloy 152 weld (Fig. 8b), and the location where some IG growth into the weld was detected (Fig. 8c). Again, the preferred SCC propagation direction is along the dendritic grains, but unfortunately this does not coincide with the test plane.

In summary, the two cross sections show that while the LAS-Alloy 152 interface is a preferred path for fatigue crack propagation, it appears to be highly resistant to SCC. In fact, in this test, the crack had ample opportunity to propagate along the interface, but turned towards the weld during each attempted transition to IG SCC.

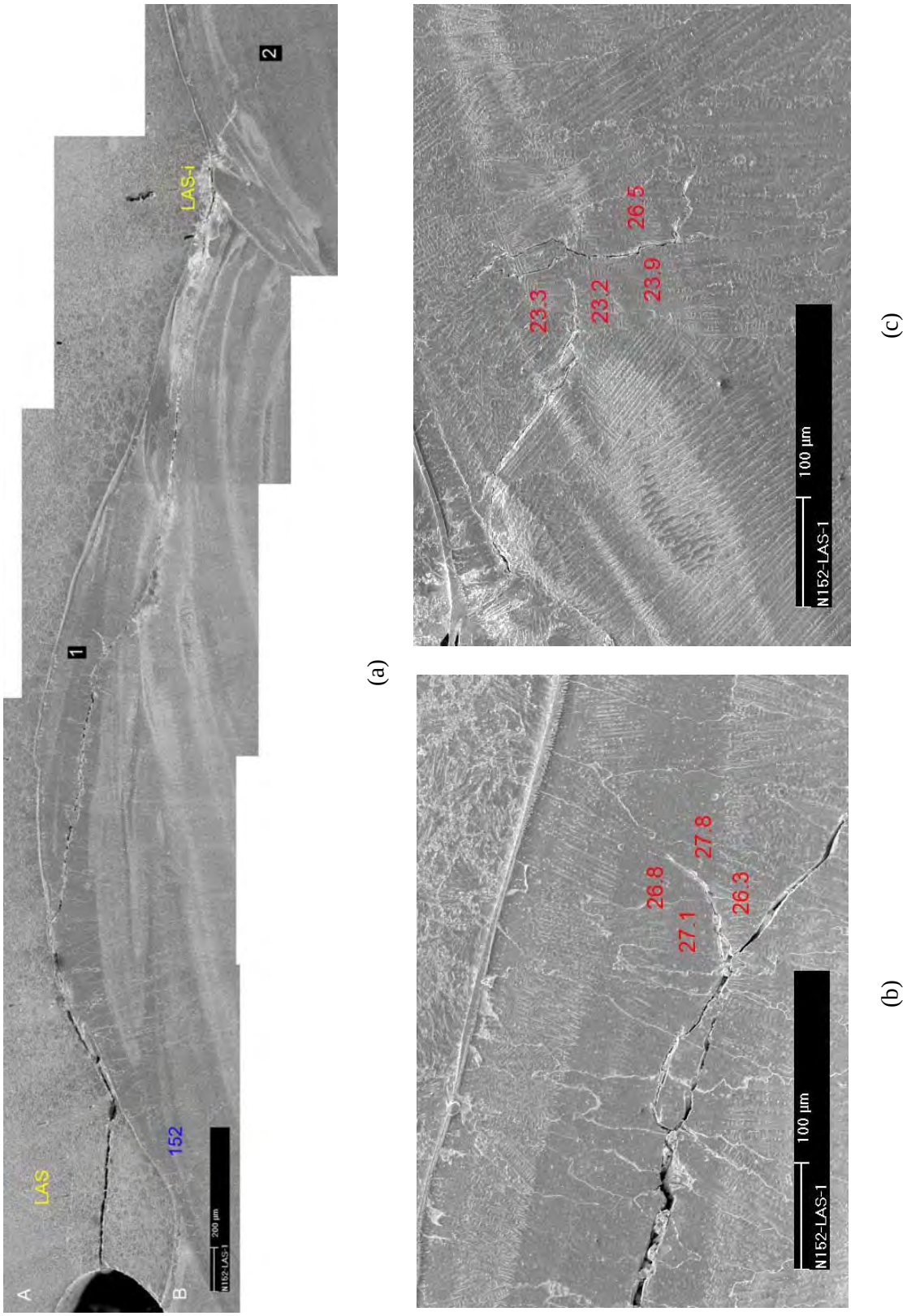

Figure 7. (a) Cross section 1 of Specimen N152-LAS-1: (a) (b) detail at location 1, and (c) detail at location 2. The local Cr concentration is shown in red. Crack advance is from left to right.

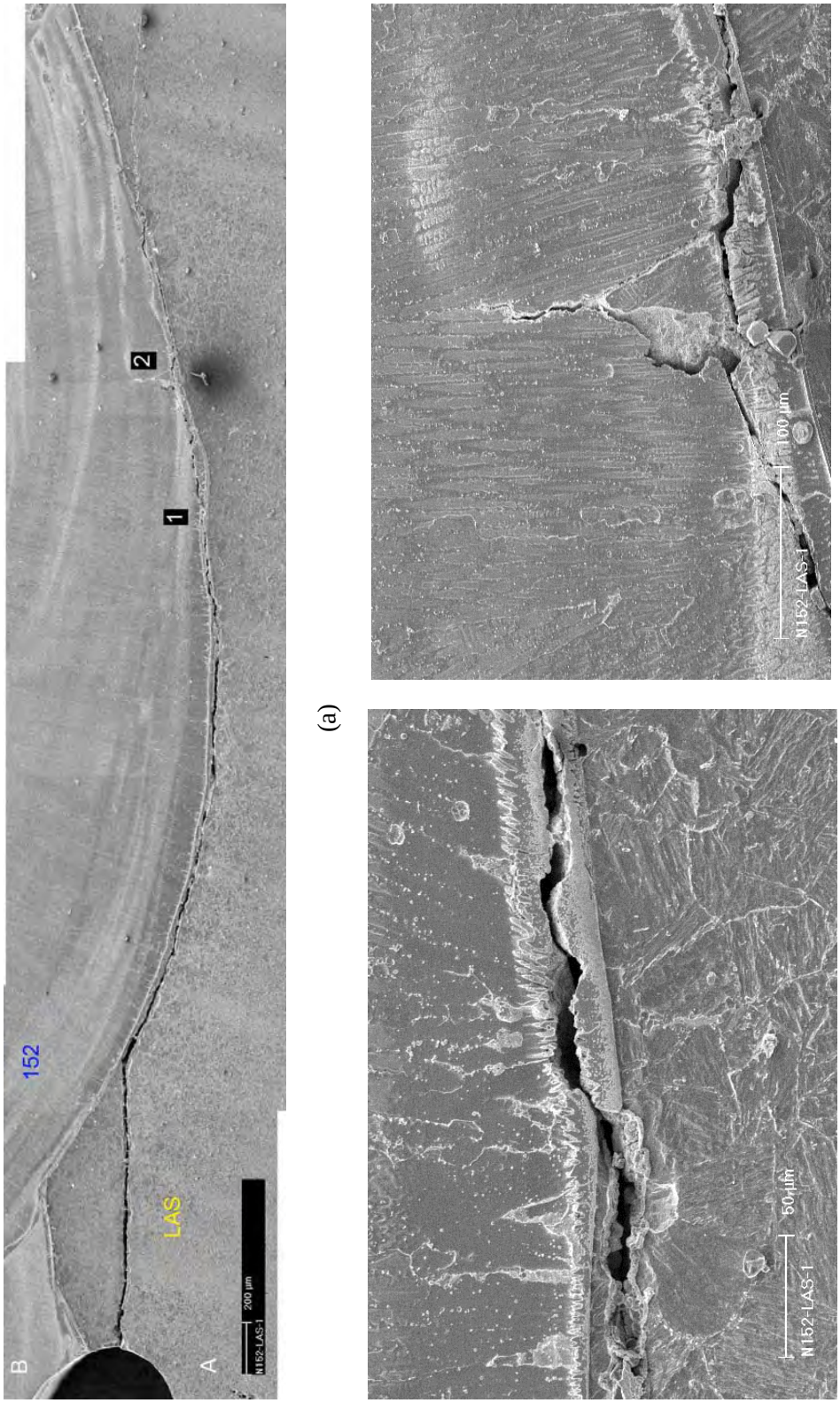

Figure 8. (a) Cross section 2 of Specimen N152-LAS-1: (a) (b) detail at location 1, and (c) detail at location 2. Crack advance is from left to right.

Next, the specimen was broken open to allow for the examination of the fracture surface, Fig. 9. The major landmarks of the test are indicated in the figure. As described previously (Fig. 7), the crack started in the LAS, propagated along the interface and into the weld (note that there is no difference in appearance between the interface and the weld), and the first set of SCC CGR determination were made at location IG-1. Then, the crack was advanced through the weld, transitioned to IG SCC, hit the LAS interface again at location marked LAS-i, then continued its advance in an IG/interdendritic mode in the weld, IG-2. Rather large ligaments were observed on the left hand side of the fracture surface that developed during fatigue and corrosion fatigue propagation through the weld. It should be noted that for Fig. 9 the fracture surface was photographed slightly tilted to show the full extent of IG-2 and ligaments (marked with red arrows) that developed in that region.

Measurements performed on the un-tilted the fracture surface yielded an overall measurement error of 39%, and because ligaments have been observed in all stages of the test, this correction was applied uniformly along the DC potential data set. However, it is important to observe that especially in the tilted photograph (Fig. 9), the extent of IG-2 appears to be approx. 5 times higher than the crack advance of 0.3 mm measured by DC potential for this region where the crack propagated off-plane. Hence, one conservative way to evaluate the SCC CGR for the entire region would be to simply divide the full extent of the crack by the time, and obtain approx. 5 10^{-11} m/s.

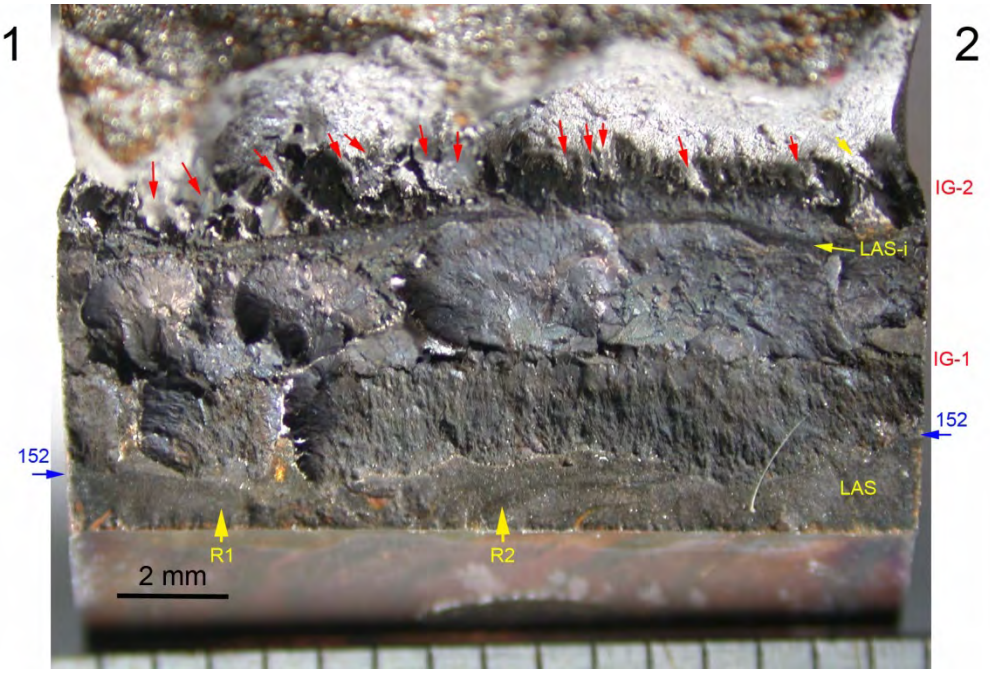

Figure 9. Fracture surface (A, Fig. 8) of specimen N152-LAS-1 tilted to show the final IG region. Crack advance is from bottom to top.

Figure 10 shows an image obtained in region R2 of Fig. 9. This image identifies the transition from LAS to Alloy 152 with blue arrows, and two additional locations of interest: IG-1 (location 1) and the second intersection of the crack with the LAS interface (location 2), labelled LAS-i. These locations are shown at higher magnification in Fig. 11. In region IG-1, while the crack propagated mostly off-plane, a somewhat uniform IG/interdentritic mode (normal to the plane of the picture) can be observed, Fig. 11a. Figure 11b focuses on the intersection with the LAS at location 2 in Fig. 10. Again, one observes that what appears to be a fully engaged IG crack in the weld does not propagate into the LAS, but somehow manages to continue as an IG crack in the weld after it reaches the weld again at the top of the picture. Such areas would have likely remained as un-broken ligaments if the crack was not advanced under cyclic loading.

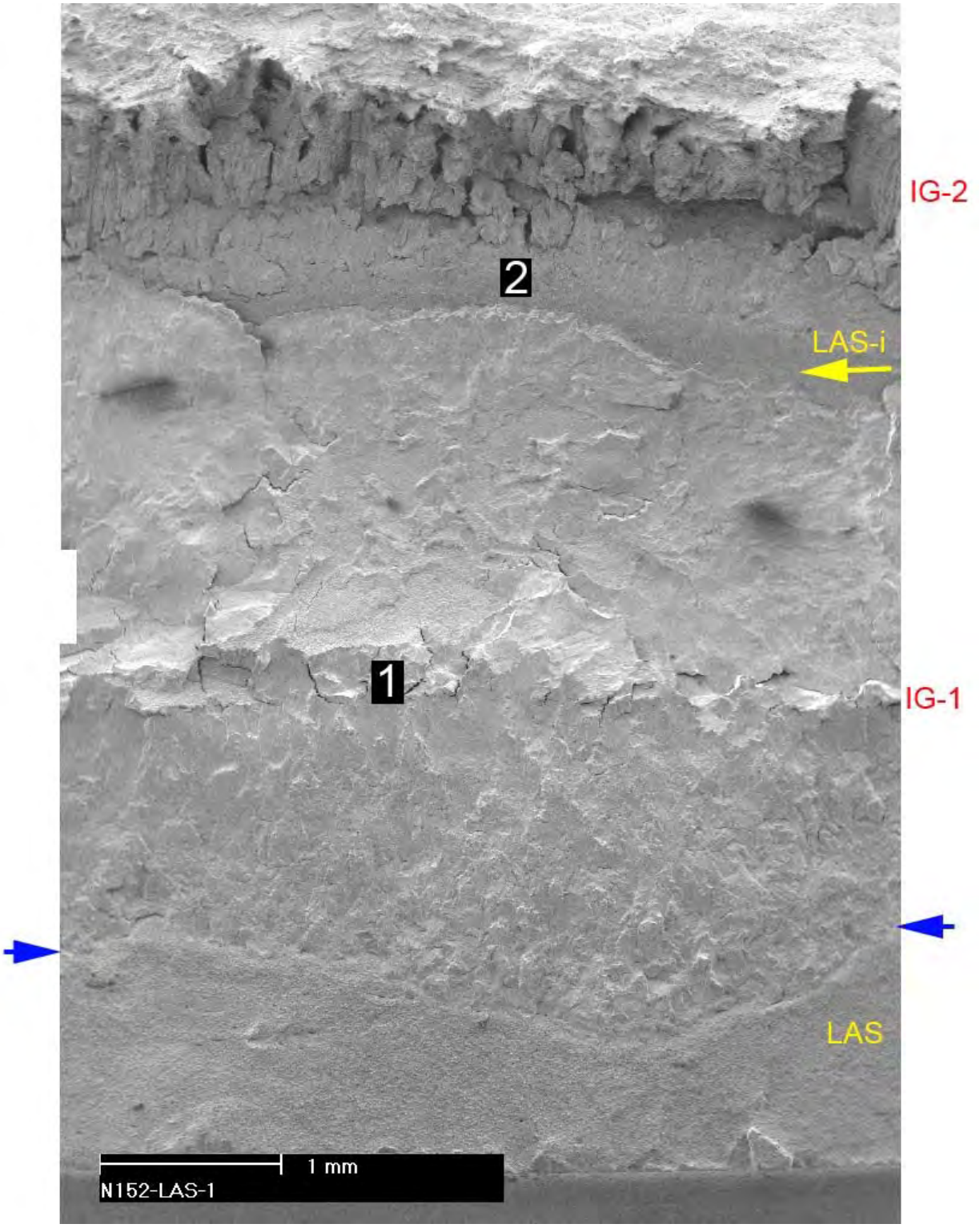

Figure 10. Region R2 on the fracture surface A of specimen N152-LAS-1 (Fig. 9). Blue arrows indicate the transition from LAS to Alloy 152, and two additional locations of interest: IG-1 (location 1) and the second intersection of the crack with the LAS interface (location 2), labelled LAS-i. Crack advance is from bottom to top.

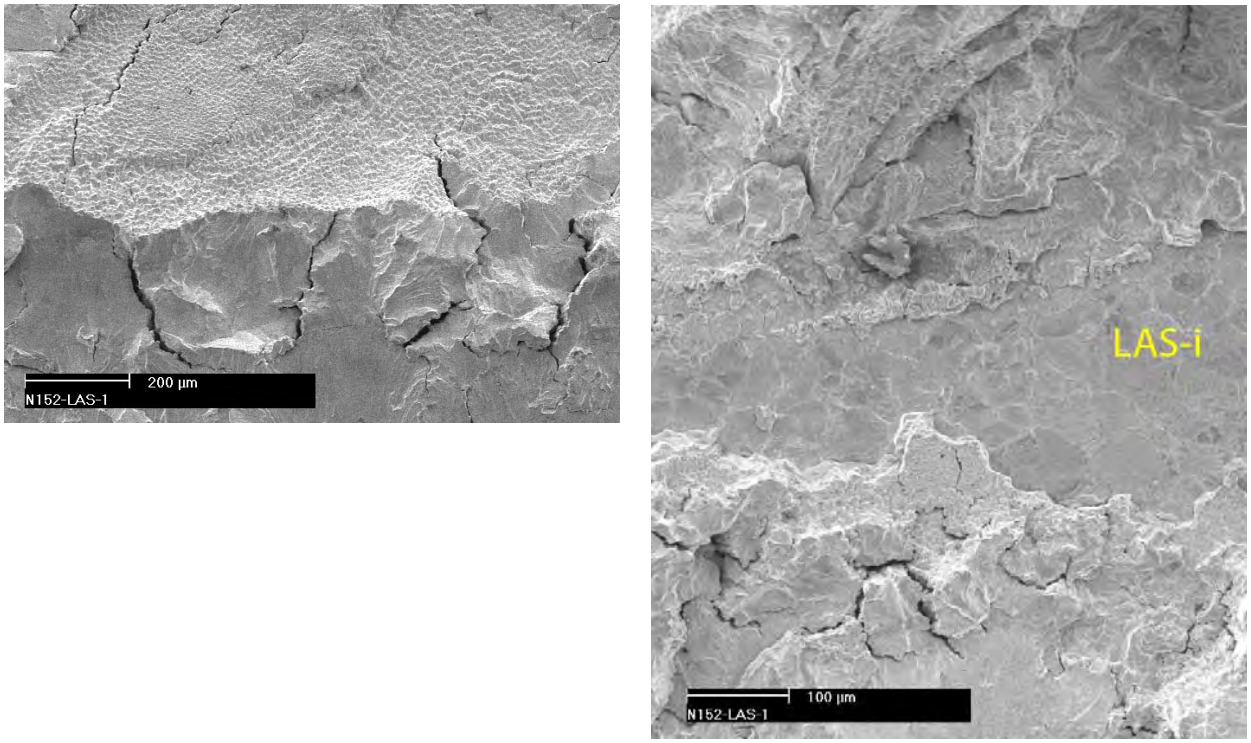

(a) (b)

Figure 11. Fracture surface of specimen N152-LAS-1, locations: (a) 1, and (b) 2 in region R2, Fig. 10. Crack advance is from bottom to top.

Figures 12 and 13 focus on region IG-2 (Fig. 9), and in order to show some detail, the fracture surface was broken down into two halves. Areas of interest are identified in both pictures. As such, Fig. 12b shows the IG interdendritic cracking observed at location 1 in Fig. 12a, and Fig. 12c focuses on a large ligament observed at location 2, also in Fig. 12a. Figure 12c also indicates the interaction between the crack and the LAS interface, L2. As noted previously, one observes that what appears to be a fully engaged IG crack in the weld does not propagate into the LAS, but manages to continue as an IG crack in the weld after it reaches the weld again at the top of the picture. It is likely that this area would have remained as an un-broken ligament if not for the cyclic loading. Likewise, Fig. 13 shows the second half of region IG-2 (Fig. 9). Figure 13b shows the IG interdendritic cracking observed at location 3 in Fig. 13 a, and Fig. 13c focuses on a large ligament and surrounding IG cracking observed at location 4 in Fig. 13 a. Overall, the fracture mode in the IG-2 region was almost completely IG. However, as noted previously, the direction of propagation was off-plane, and, hence, there should be no surprise that the DC potential recorded very low or "no growth" SCC SGRs.

In summary, the conclusions and, more importantly", the "lessons learned" from the first test are as follows:

- The Cr-diluted Alloy 152 butter is susceptible to SCC, the IG fracture mode was found to occur readily, and the measured SCC rates are high enough to warrant further investigation. However, cracking tends to occur off-plane, hence, constant load should follow quickly once a "susceptible" region is identified. This could be accomplished by eliminating the test periods with a hold.
- The LAS and LAS-Alloy 152 interface is resistant to SCC. As such, to avoid crack arrest at the LAS-152 interface, future specimens should be aligned further away from the Alloy 152-LAS interface.

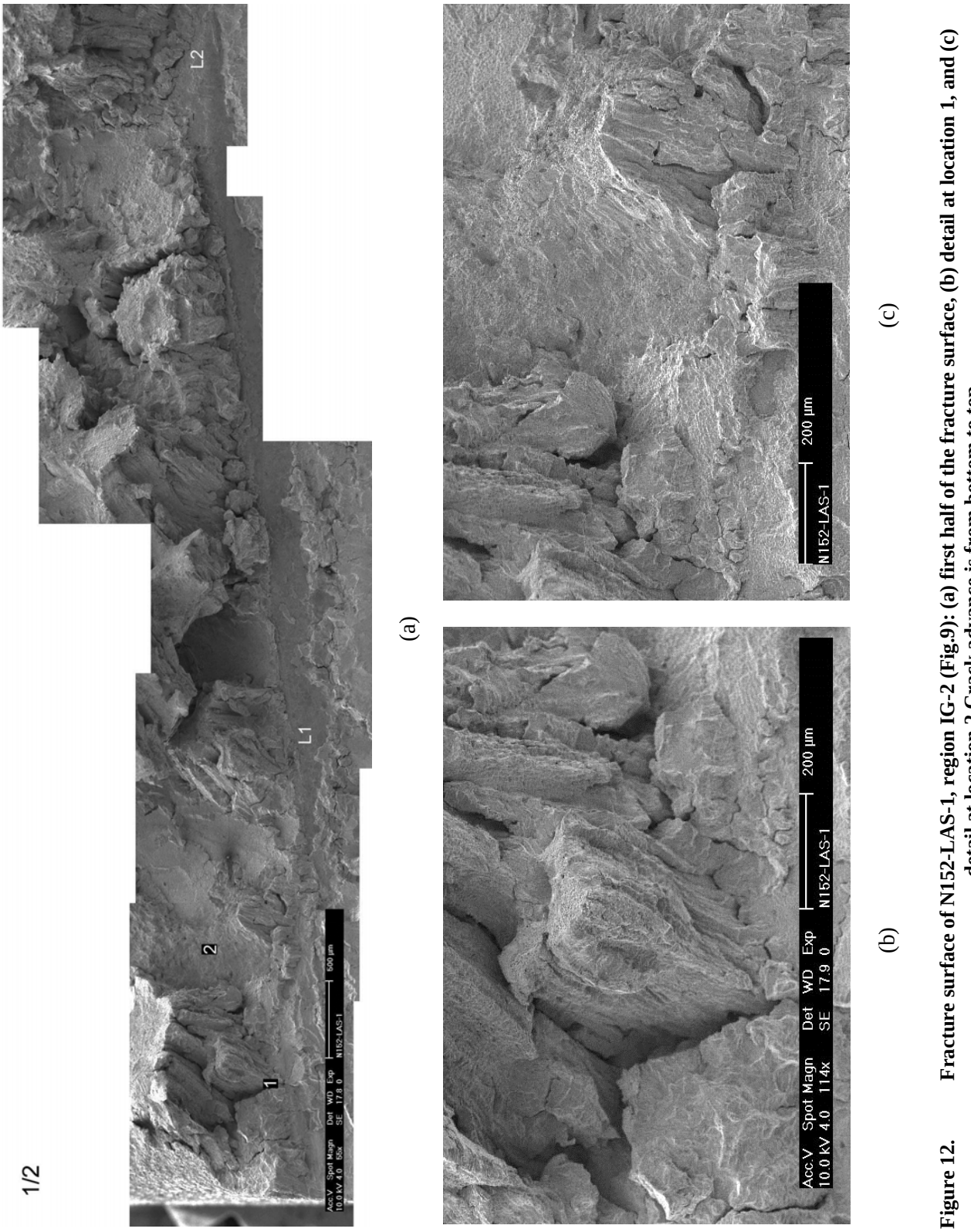

Figure 12. Fracture surface of N152-LAS-1, region IG-2 (Fig.9): (a) first half of the fracture surface, (b) detail at location 1, and (c) detail at location 2.Crack advance is from bottom to top.

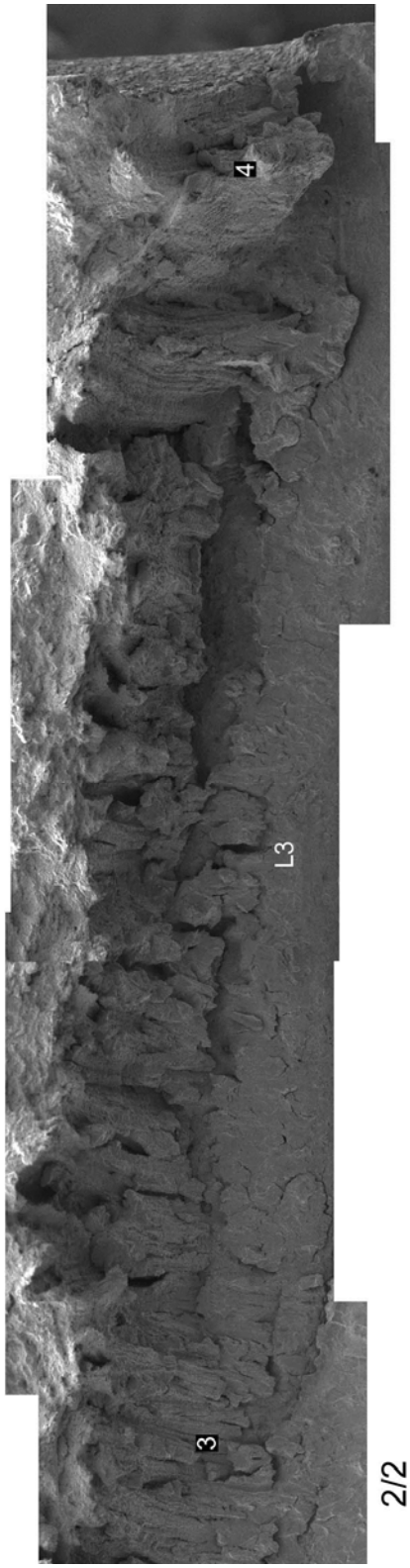

(a)

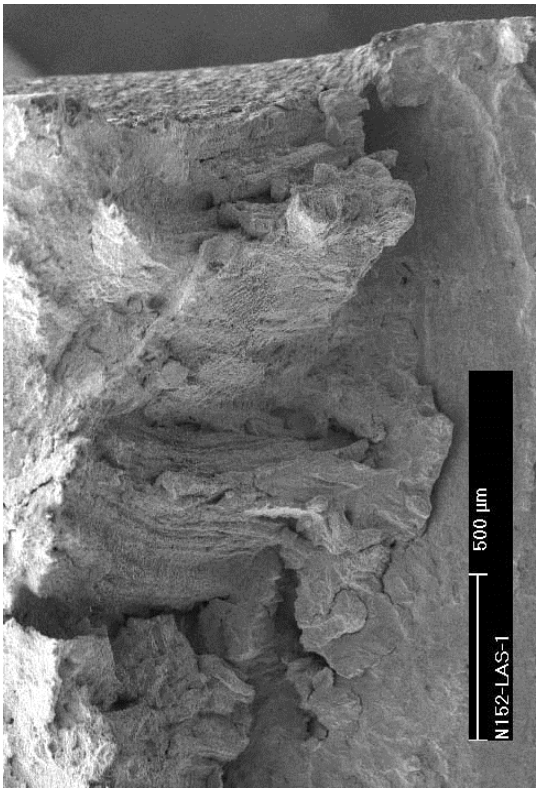

(c)

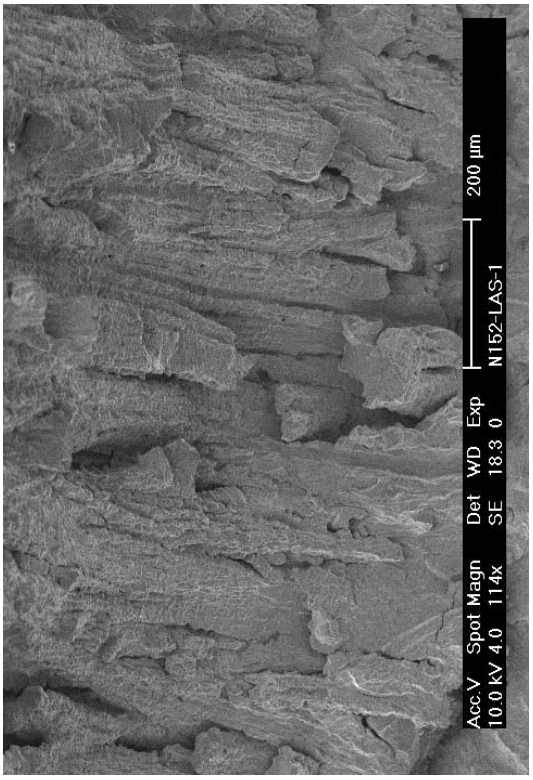

(b)

Figure 13. Fracture surface of N152-LAS-1, region IG-2 (Fig.9): (a) second half of the fracture surface, (b) detail at location 3, and (c) detail at location 4. Crack advance is from bottom to top.

3.2 SCC CGR test on 1st Layer Alloy 152 weld butter Specimen N152-LAS-11

The second test benefitted from the "lessons learned" in the first test. As such, in order to avoid crack interaction and arrest at the Alloy 152-LAS interface, the notch of Specimen N152-LAS-11 was still machined in the 1st layer of Alloy 152 weld, but further away from the interface with the LAS, Fig. 14.

(a) (b)

Figure 14 The two sides of specimen N152-LAS-11 prior to the SSC test: (a) side 1, and (b) side 2. Alloy 152 is in the top half, and the LAS is in the bottom half of both pictures.

The test on specimen N152-LAS-11 was initiated with precracking in the PWR environment, followed by transitioning. The testing conditions are given in Table 4, and a visual representation of the test in the framework described previously is shown in Fig. 15. As before, the plots tracks the environmental enhancement of two loading conditions – rise 50s and rise 600s, R = 0.5 – vs. crack advance from the notch. The purpose of the fast cycle is to advance the crack, and the purpose of the slow cycle is to probe for environmental enhancement. The dotted red and blue horizontal lines represent the enhancement levels of a forward advancing crack based on the prior Alloy 152 experience (Fig. 2).

Early data (Fig. 15) seem to show an environmental enhancement exceeding the highest that was observed in the N152-LAS-1 specimen (and in the Alloy 152 tested previously, Fig. 2), hence, the current specimen was set at constant load fairly early in test period 4. Upon measuring a small SCC CGR, the cyclic routine was repeated, allowing more time in test period 6 to assess the SCC CGR component. Based on superposition in test periods 5 and 6, this was calculated to be 1.7×10^{-12} m/s. The rate was next measured at constant load in test period 7 and was found to be indeed very small, 1.4×10^{-12} m/s. Subsequent cycling in test period 8 found significantly less environmental enhancement (Fig. 15). The dramatic drop in cyclic response suggests that SCC occurred off-plane, and the SCC CGR measurements conducted in the interim are perhaps of little significance.

Next, the crack was advanced incrementally using the fast/slow loading conditions described previously, monitoring the environmental enhancement in an attempt to identify another "SCC-susceptible" microstructure. A condition yielding comparable enhancement to that resulting in a 1.81×10^{-11} m/s SCC CGR in the prior test was identified in test period 27. Next, the test was converted directly to constant load in test period 18, assuming that the more susceptible material was at that point still ahead of the crack. The test ended after approx. 2,700h in this condition resulting in approx. 1.4 mm of growth (after a

factor 10 correction based on the fracture surface was applied to the DC potential data), Fig. 16. While the average SCC CGR was approx. 1.4×10^{-10} m/s, the rate was observed to accelerate locally to rates as high as 3.1×10^{-10} m/s, and slow down to rates as low as 4.0×10^{-11} m/s. In summary, there are two regions in this specimen, i.e., test periods 7-14 and 28, with SCC CGRs differing by a factor 100, and the subsequent post-test examination will have to elucidate the reason for the difference.

Table 4. Crack growth data for Alloy 152 dilution specimen N152-LAS-11 in PWR water[a].

Test Period	Test Time, h	Temp. °C	Load Ratio R	Rise Time, s	Down Time, s	Hold Time, s	K_{max}, MPa·m$^{1/2}$	ΔK, MPa·m$^{1/2}$	CGR_{env}, m/s	Estimated CGR_{air},[b] m/s	Crack Length, mm
Pre a	55	320.0	0.30	1	0.5		22.8	15.9	2.26E-08	8.75E-08	11.784
Pre b	71	320.0	0.30	50	50		22.9	16.0	1.24E-09	8.98E-10	11.819
Pre c	74	319.8	0.30	1	0.5		23.5	16.5	5.17E-08	1.00E-07	12.029
1	78	320.5	0.50	50	12		23.5	11.7	8.74E-10	4.33E-10	12.043
2	143	319.9	0.50	600	12		23.6	11.8	1.41E-10	3.66E-11	12.076
3	176	319.9	0.50	600	12	7,200	23.6	11.8	2.43E-11	2.83E-12	12.084
4	493	320.0	1.00	0	0		23.7	0.0	5.34E-12	-	12.095
5	504	320.1	0.50	600	12		23.8	11.9	1.60E-10	3.76E-11	12.104
6	912	320.1	0.50	600	12	7,200	23.8	11.9	1.89E-11	2.92E-12	12.131
7	1,442	320.1	1.00	0	0		23.7	0.0	1.47E-12	-	12.131
8	1,488	320.1	0.50	600	12		23.6	11.8	9.78E-11	3.65E-11	12.145
9	2,067	320.1	0.50	600	12	7,200	23.5	11.8	1.42E-11	2.78E-12	12.181
10	3,026	320.1	1.00	0	0		23.8	0.0	1.25E-12	-	12.189
11	3,864	320.0	0.50	12	12	14,400	24.0	12.0	3.67E-12	1.64E-12	12.204
12	3,888	320.1	0.50	600	12		26.9	13.4	1.68E-10	6.26E-11	12.216
13	4,009	320.2	0.50	600	12	7,200	27.0	13.5	2.81E-11	4.90E-12	12.233
14	5,713	320.1	0.50	12	12	28,800	27.3	13.6	4.87E-12	1.38E-12	12.265
15	6,025	320.2	0.50	600	12	-	27.6	13.8	1.20E-10	6.98E-11	12.374
16	6,049	320.1	0.50	50	12		27.8	13.9	1.23E-09	8.63E-10	12.458
17	6,239	320.2	0.50	600	12		28.3	14.2	1.50E-10	7.76E-11	12.560
18	6,287	320.2	0.50	50	12		27.9	14.0	1.13E-09	8.77E-10	12.700
19	6,365	320.3	0.50	600	12		28.2	14.1	1.53E-10	7.61E-11	12.742
20	6,408	320.1	0.50	50	12		28.2	14.1	1.54E-09	9.08E-10	12.901
21	6,528	320.2	0.50	600	12		28.7	14.3	1.84E-10	8.13E-11	12.982
22	6,550	320.3	0.50	50	12		29.0	14.5	1.41E-09	1.03E-09	13.073
23	6,597	320.2	0.50	600	12		29.3	14.6	1.90E-10	8.84E-11	13.106
24	6,621	320.3	0.50	50	12		29.8	14.9	1.48E-09	1.15E-09	13.208
25	6,699	320.1	0.50	600	12		30.1	15.1	2.35E-10	9.97E-11	13.273
26	6,718	320.1	0.50	50	12		30.4	15.2	1.76E-09	1.23E-09	13.362
27	6,743	320.0	0.50	600	12		30.7	15.3	2.79E-10	1.07E-10	13.374
28	9,417	320.2	1.00	0	0		37.9	0.0	1.42E-10	-	14.728

[a]Simulated PWR water with 2 ppm Li, 1000 ppm B, and 2 ppm. DO<10 ppb. Conductivity was 21±3 µS/cm, and pH 6.4.
[b]CGR rates in air are calculated assuming typical behavior for a Ni-base weld. The 152-LAS rates are approx. a factor 2 lower.

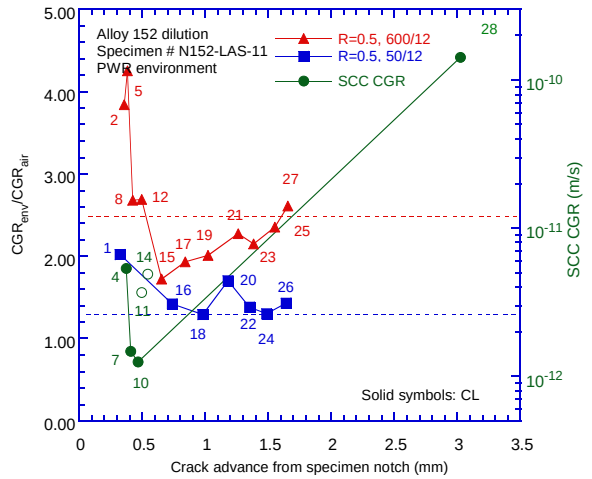

Figure 15. Environmental enhancement of two control test conditions and SCC CGRs vs. distance from the specimen notch for Specimen N152-LAS-11. Test periods are indicated in the figure.

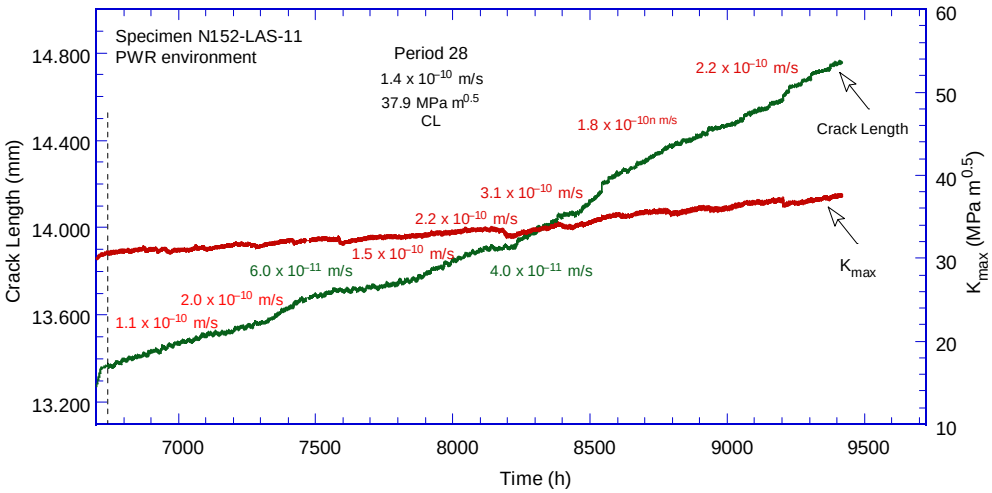

Figure 16. Crack–length–vs.–time for specimen N152-LAS-11 under constant load in simulated PWR environment in test period 28. Local SCC CGRs are also indicated in the figure.

After the test was completed, the sample was removed from the autoclave and the side surfaces were ground to remove the side grooves. No fatigue in air was done immediately following the completion of the test in water in order to be able to establish precisely on the side surfaces where the test ended. The images shown in Fig. 17 indicate that the test started and ended in the 1st layer of Alloy 152.

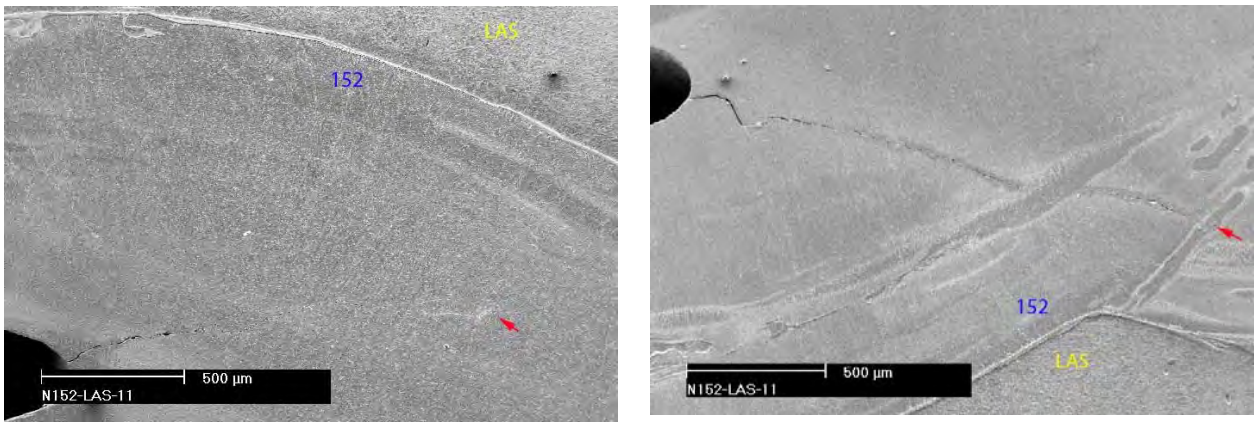

(a) (b)

Figure 17. SEM images of the two sides of the dilution specimen N152-LAS-11 after the test: (a) side 1, and (b) side 2. Alloy 152 and the LAS are as marked in each picture. The red arrows mark the end of the test.

The side surfaces were examined in the SEM to investigate the difference in cracking between the regions in this specimen with SCC CGR differing by a factor 100, namely between test periods 7-14 and 28. Side surface 1, Fig. 17a, does not seem to provide much revealing information. By contrast, side surface 2, Fig. 17b, appears to shows some detail at the locations of interest. As such, Fig. 18 identifies the regions of low SCC CGR (location 1) and high SCC CGR (location 3). The average composition (wt. %) at location 1 (Fig. 18b) is 26.1 Cr - 24.4 Fe - 49.5 Ni, and the average composition (wt. %) at location 3 (Fig. 18c) is nearly identical, 25.4 Cr – 26.6 Fe – 48.0 Ni. Hence, the chemical composition does not seem to account for the apparent factor 100 difference in SCC CGRs. However, SCC at location 1 (Fig. 18b) is clearly off-plane; hence, the low SCC CGRs measured by DC potential at this location could be due to off-plane cracking.

Of high interest was also the interaction of the crack front with the two "streaks" shown at locations 2 and 3 in Fig. 18a. At closer inspection, Fig. 19, these seem to either slow (location 2) or arrest (location 3) the crack advance. The average composition (wt. %) for the "streaks" was 19 Cr – 44 Fe – 36 Ni, hence, a low Cr concentration does not seem to necessarily translate into an increased SCC-susceptibility.

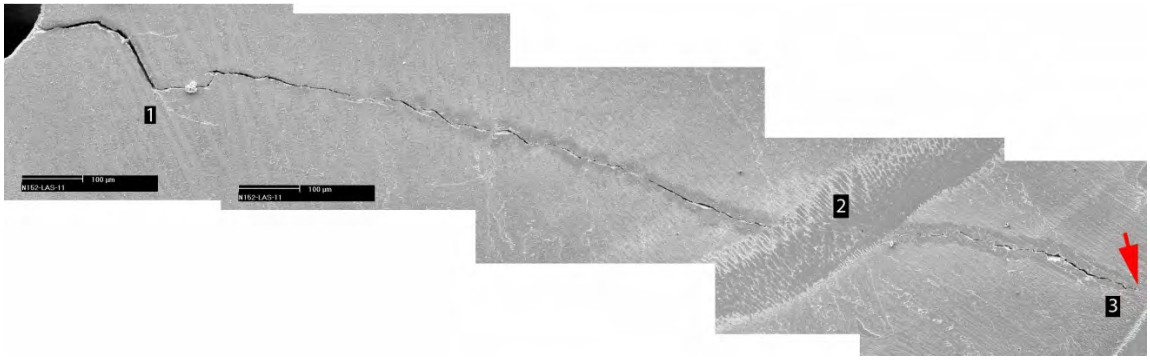

(a)

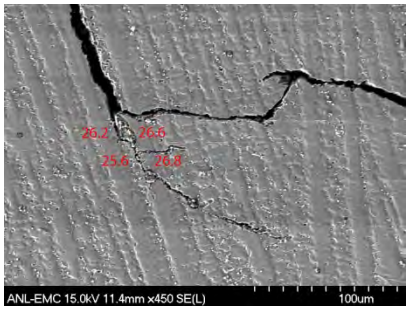

(b)

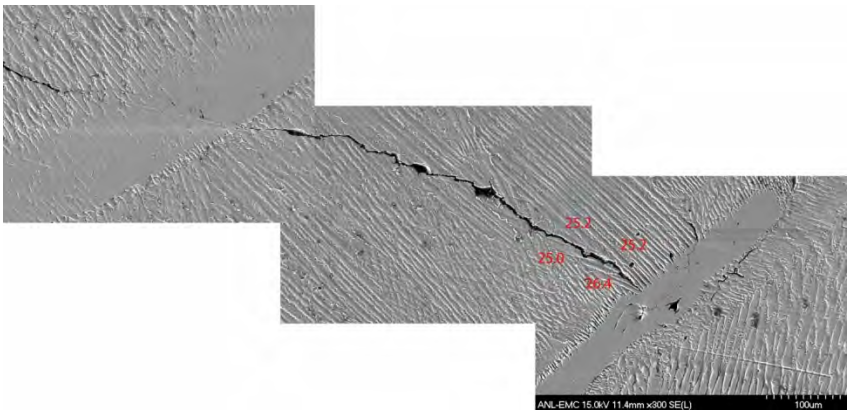

(c)

Figure 18. (a) Side surface 2 of Specimen N152-LAS-11; Regions with low (b) and high (c) SCC CGRs as observed on the side surface "2" at locations 1 and 3. Local Cr concentration (wt. %) measurements are indicated with red in each figure. Crack propagation is from left to right.

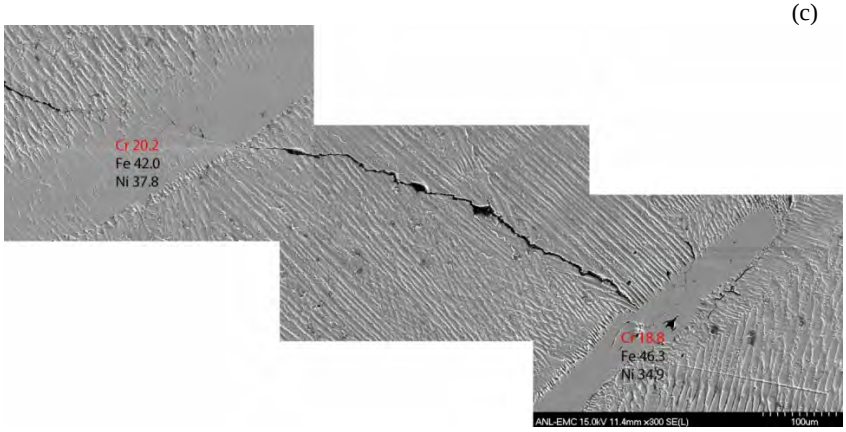

Figure 19. "Streaks" appearing to slow down/arrest crack propagation observed on the side surface 2 in specimen N152-LAS-11 (locations 2 and 3 in Fig. 18b). Measured Cr concentration (wt. %) for each "streak" is indicated with red in the figure. Crack propagation is from left to right.

After the examination of the side surfaces, the specimen was fatigued in air for an additional 2 mm, and then broken open to examine the fracture surface, Fig. 20. The milestones of the test are indicated in the figure: the specimen was set at constant load fairly early in the test (IG-1), then the crack was advanced by cyclic loading (test periods 15-27, Table 4), and finally the specimen was set at constant load in test period 28. Advance under cyclic loading produces a relatively straight fracture surface with no ligaments, and this is especially true for test period 27 which reproduced the expected CGR for Alloy 152 (Fig. 15). Hence, the red lateral arrows in Fig. 20 indicate the end of cyclic loading (including test period 27). Finally, the last test period 28 produced the region labeled IG-2. This region was measured to be on average 10 times higher than the DC potential measurement of 0.140 mm, and hence, the correction for the DC potential data in test period 28 was a factor 10. The general appearance in the later part of the test – with several unbroken ligaments – was unexpected, and these areas were investigated further as it will be documented later in this section.

Figure 20 also shows the local Fe concentrations of several of the unbroken ligament regions, confirming that these regions are the result of crack interaction with the SCC-resistant Alloy152-LAS interface. These resistant regions were not suspected initially to be LAS because the post-test examination of the side surfaces (Fig. 17) suggested that the crack was contained in the Alloy 152 weld. Nevertheless, there appears that, unlike the previous specimen where the crack was advanced with gentle cycle + hold and constant load with periodic unloading and overcame the LAS regions, in the current specimen under constant load the areas where the crack interacted with the LAS remained as unbroken ligaments. However, it seems that the crack found a path around those regions, and appeared to propagate as long as there was weld metal available. Overall, the fracture surface suggests that the crack was eventually arrested at the intersection with the LAS on the left side, but propagated quite extensively in the weld on the right side. Given the extent of the unbroken ligaments, the large correction factor was not surprising.

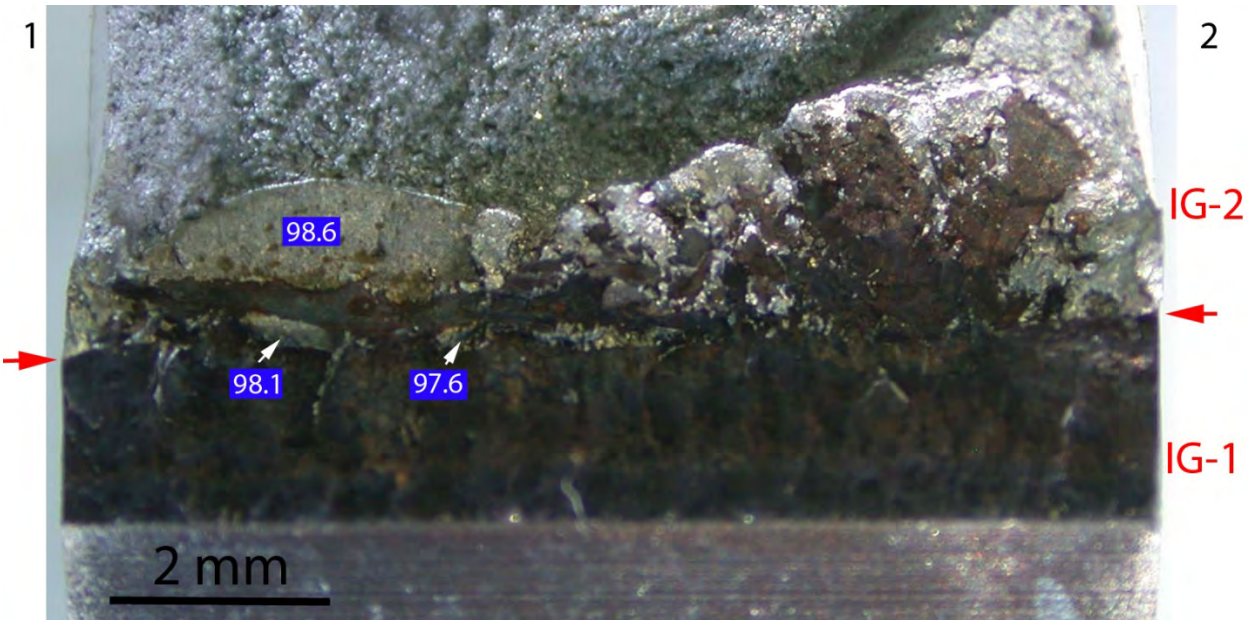

Figure 20. Fracture surface of specimen N152-LAS-11. The red lateral arrows indicate the end of cyclic loading and the beginning of the final constant load test period. Measured Fe concentration (wt. %) for at several locations is indicated with red in the figure. Crack advance is from bottom to top.

Figure 21 shows the entire fracture surface of specimen examined in the SEM. Additional images at areas of interest were acquired and will be discussed next.

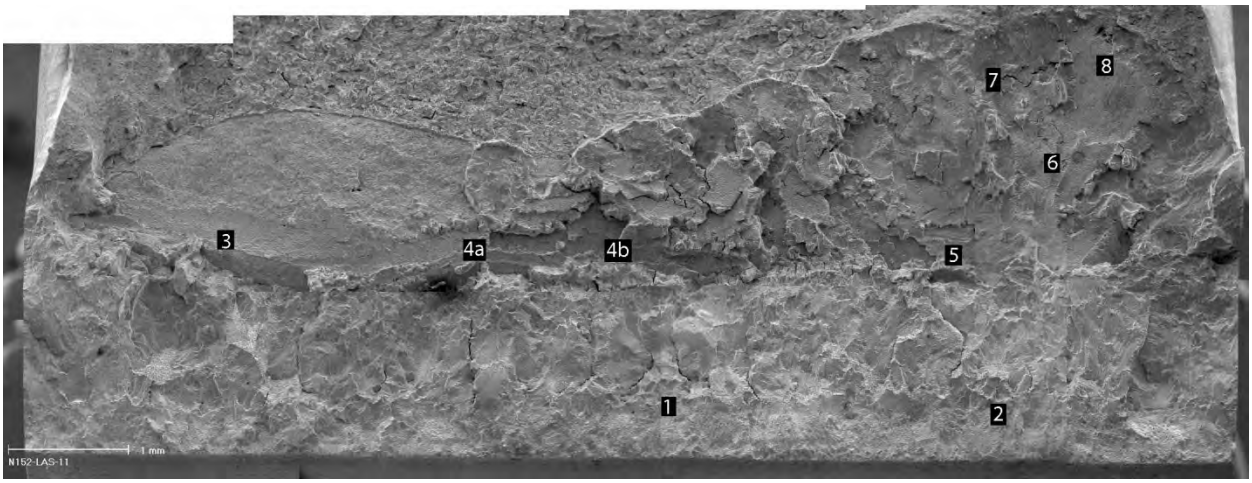

Figure 21. Fracture surface of specimen N152-LAS-11. Crack advance is from bottom to top.

Figure 22 focuses on what was believed to be (based on the DC potential measurement) the SCC-resistant region IG-1 (location 1 in Fig. 21). The presence of IG fracture very early in the test explains the high environmental enhancement observed in test periods 2, and 5 (Fig. 15). Eventually, the environmental enhancement is lost as the preferred crack direction is off-plane. The fracture mode for this region appears on the fracture surface as mixed IG-TG mode, with extensive secondary (off-plane) cracking.

Figure 23 illustrates the interaction of the crack front with the LAS (locations 3 and 4b in Fig. 21). As described previously in the context of discussing Fig. 20, these regions are resistant to SCC, and remained as un-broken ligaments on the fracture surface under constant load conditions. The crack eventually found a path around them and propagated as long as there was weld metal available.

Figure 24 shows two locations from the final part of the test (7 and 8 in Fig. 21). Propagation is in an IG mode, in a direction perpendicular to the direction of the dendrites, and in a finger-like manner that leaves unbroken ligaments behind. Overall, a similar fracture mode was observed in 1st layer of Alloy 52M deposited on an Alloy 182 interface.[5]

Finally, in order to obtain additional confirmation on the crack path, the test specimen was further sectioned along directions “11” and “22”, as shown schematically in Fig. 25. Cross section “11” was chosen in an area where the crack was arrested at the LAS, and cross section “22” was chosen in an area where the crack propagated over several millimeters. Figure 25b indicates that the crack observed on cross section “11” was indeed arrested at the interaction with the LAS and, along with Fig. 25a and Fig. 23a, demonstrates that the crack continued to propagate as long as there was some weld available. Figure 25c demonstrates that the crack observed on cross section “22” propagated freely into the Alloy 152 weld with no interference from the LAS interface.

In summary, the test on specimen N152-LAS-11 confirmed the prior observations. The 1st layer of the Alloy 152-LAS weld is susceptible, and in the second test, in a favorable orientation, a SCC CGR in the 10^{-10} m/s range was measured.

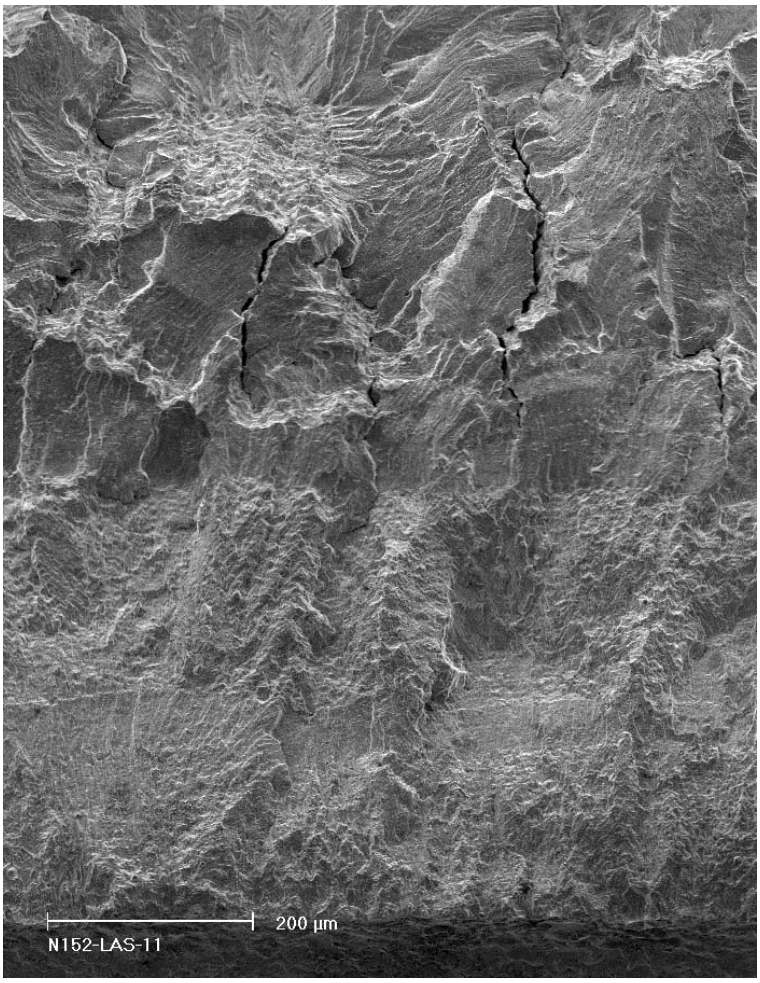

Figure 22. **Fracture surface of specimen N152-LAS-11 at location 1 in Fig. 21. Crack advance is from bottom to top.**

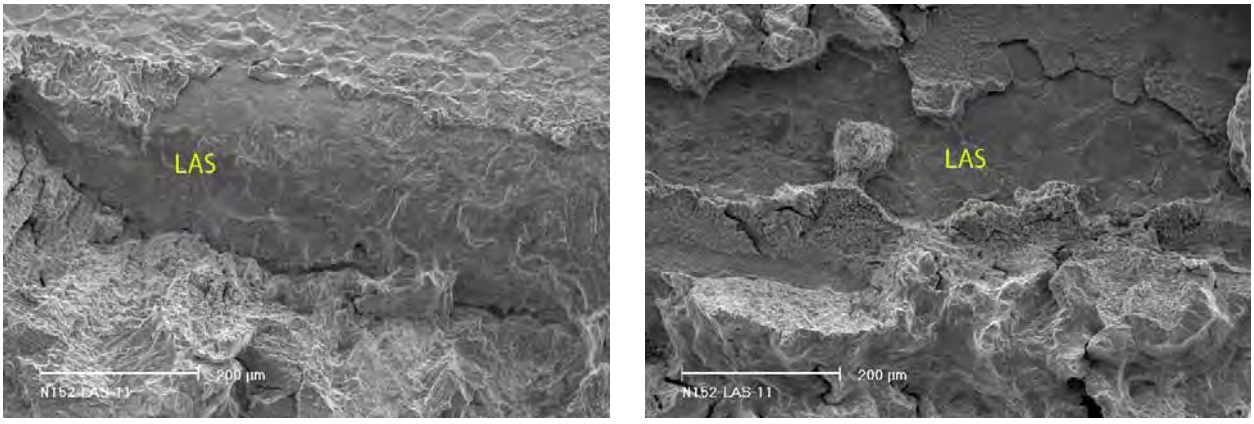

(a) (b)

Figure 23. **Fracture surface of specimen N152-LAS-11 at location: (a) 3, and (b) 4b in Fig. 21. Crack advance is from bottom to top.**

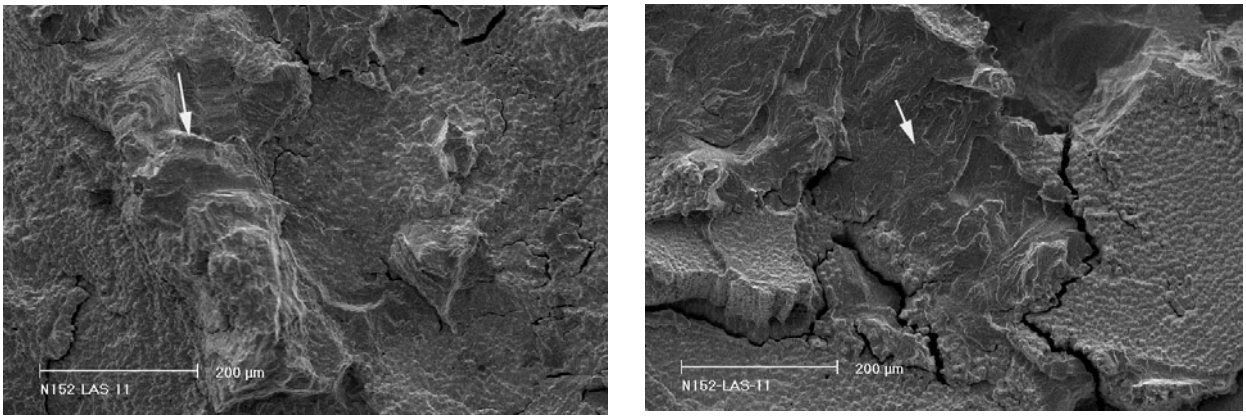

(a) (b)

Figure 24. Fracture surface of specimen N152-LAS-11 at location: (a) 7, and (b) 8 in Fig. 21. Arrows indicate unbroken ligaments. Crack advance is from bottom to top.

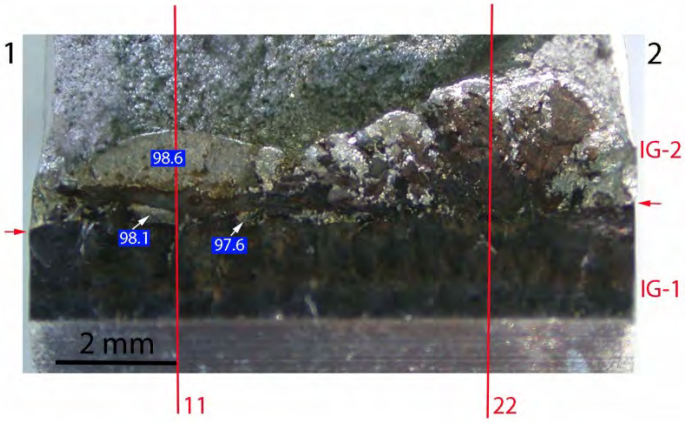

(a)

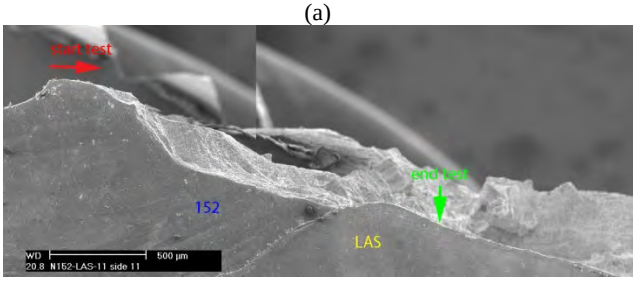

(b)

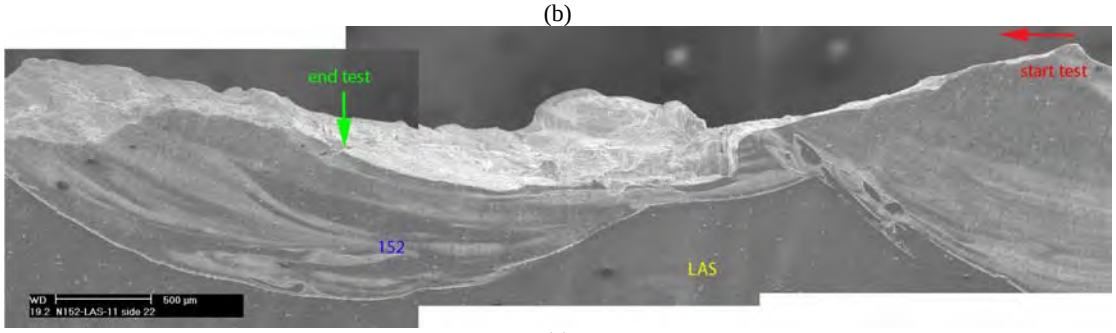

(c)

Figure 25. (a) Fracture surface of specimen N152-LAS-11. Additional cross sections were obtained along directions "11" (b), and "22" (c). Red arrows are placed at the specimen notch and indicate the direction of propagation. Green arrows indicate the end of the test.

4. DISCUSSION

This section summarizes and discusses the results for the two 1st layer Alloy 152–LAS specimens, and provides a comparison with the results obtained on the 1st layer Alloy 52M-182 specimens.[5] The effects of local Cr concentration and that of the substrate on SCC CGR response are also discussed.

4.1 1st Layer Alloy 152-LAS Cyclic and SCC CGR response

The cyclic and SCC CGRs generated in the two 1st layer Alloy 152-LAS specimens are shown as a function of distance in Fig. 26. Overall, the cyclic data for the two specimens is in excellent agreement, and the approach based on measuring the local environmental enhancement was instrumental for identifying the locations where an SCC CGR could be measured by DC potential.

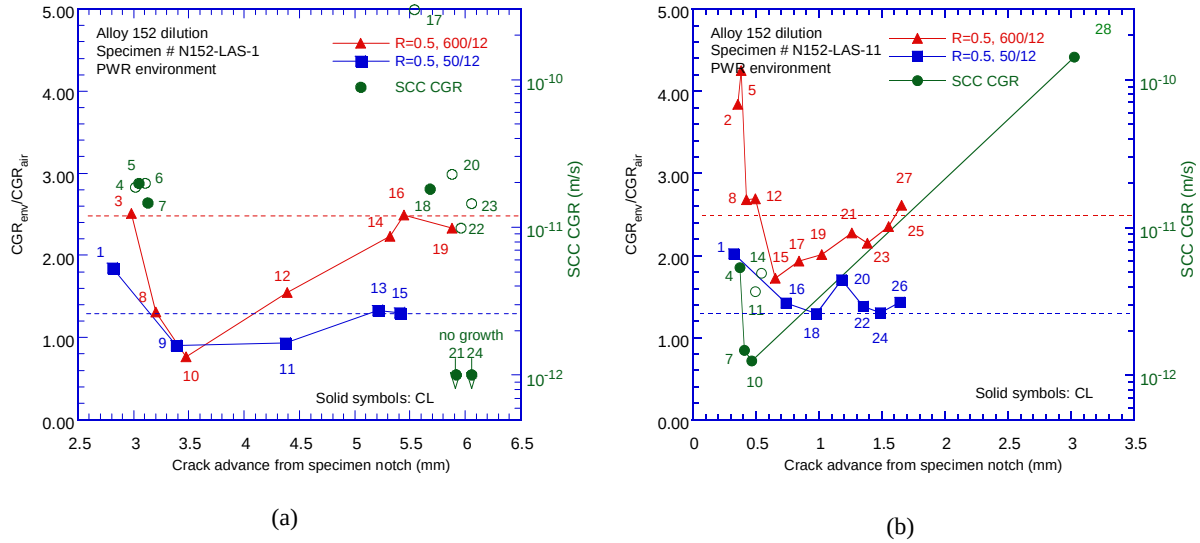

Figure 26 Environmental enhancement of two control test conditions and SCC CGRs vs. distance from the specimen notch for (a) N152-LAS-1, and (b) N152-LAS-11.

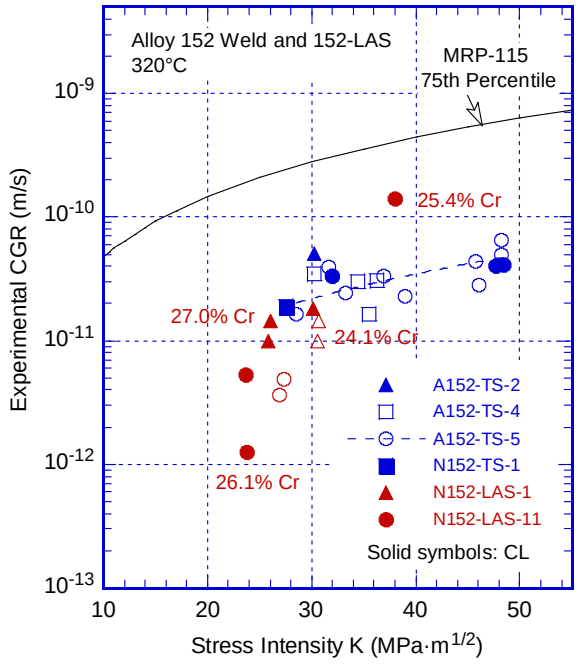

Figure 27. SCC CGRs in and 1st layer Alloy 152-LAS specimens. Also included are Alloy 152 data generated at ANL[9] and the 75th percentile MRP-115 disposition curve for Alloys 82/182.[6]

Figure 27 shows the SCC CGR data measured for the two 1st layer Alloy 152-LAS specimens along with the Alloy 152 data obtained previously on a double-J symmetrical Alloy 152 weld.[9] The Alloy 152-LAS SCC CGRs show a factor 100 variation depending on the location in the specimen where they were measured, as was already illustrated in Fig. 26. However, despite the un-favorable orientation with respect the weld dendrites, the most favorable locations of these 1st layer dilution welds can yield SCC CGRs higher than those measured for bulk Alloy 152, and within a factor 2 of the 75th percentile MRP-115 disposition curve for Alloys 82/182.[6]

4.2 Comparison of Cyclic and SCC CGR Responses in 1st Layer Alloy 152-LAS and 1st Layer Alloy 52M-182 WOL

In order to put the current 1st layer Alloy 152-LAS data into perspective, prior results obtained on 1st layer of Alloy 52M-182 WOL are included here for comparison. As such, the cyclic and SCC CGRs generated in the 1st layer Alloy 52M-182 WOL are shown as a function of distance in Fig. 28. Also, the SCC CGR data along with previous data for Alloy 152 heat WC04F6 (28.7 wt. %) tested at ANL,[9] and the MRP-115 75th percentile curve[6] are shown in Fig. 29.

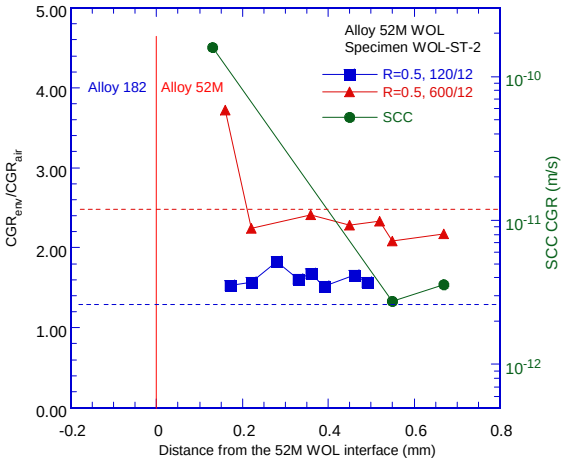

Figure 28. Environmental enhancement of two control test conditions vs. calculated distance to the interface. Crack propagation is from right to left.

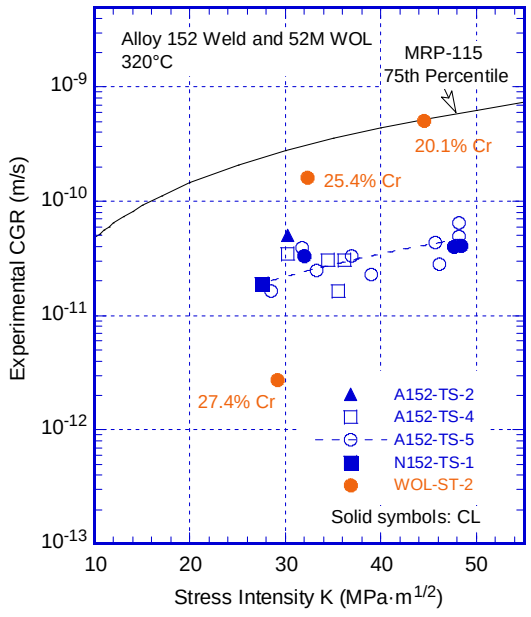

Figure 29. SCC CGRs for Alloy 52M-182 WOL specimen WOL-ST-2 as a function of average Cr content. Also included are Alloy 152 data generated at ANL[9] and the MRP-115 disposition curve for Alloys 82/182.[6]

The two sets of cyclic data (Figs. 26 and 28) are in excellent agreement, with no apparent effect from the interface or the substrate. In both cases, the environmental enhancement was a good predictor for the SCC response. Also, in both cases, in the most favorable orientations, the SCC CGRs were within a factor 2 of the MRP-115 75th percentile curve[6] (Figs. 27 and 29). As noted previously, the largest SCC CGRs were determined based on crack advances larger than 1 mm. Because of the size of these cracks, and the fact that they were readily identifiable on the fracture surface, the largest SCC CGR are deemed by the authors to be highly reliable. It is also interesting to note that in both 1-st layer welds, the propagation occurred in a direction perpendicular to the dendrites, Fig. 30. It is not clear whether this propagation mode even exists in Alloy 182 or it is specific to those high-Cr weld layers near an interface.

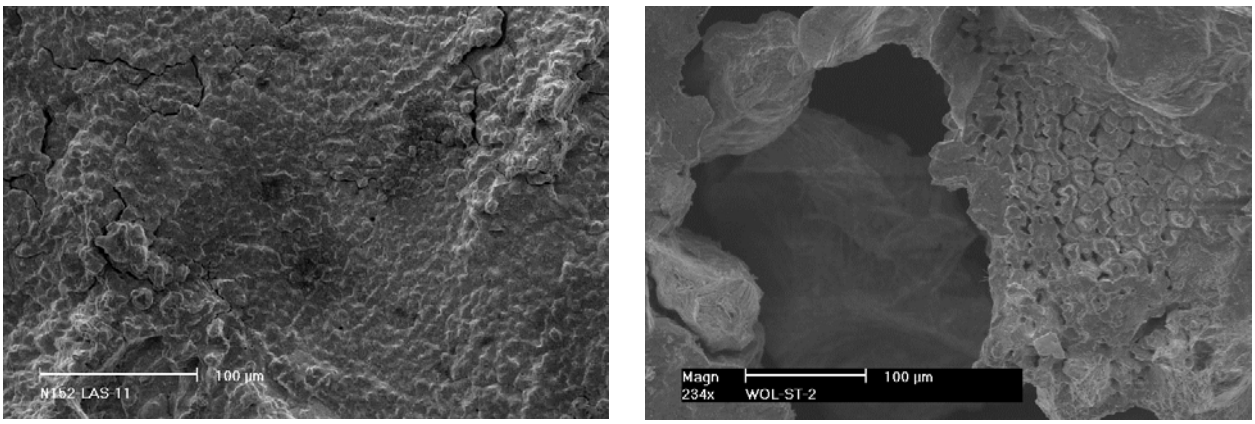

(a) (b)

Figure 30 SCC fracture modes the regions near the interface in (a) Alloy 152 – LAS, and (b) Alloy 52M WOL specimens tested in simulated primary water environment. SCC propagation is from bottom to top.

4.3 The Effect of Local Cr concentration and that of the Substrate on the Cyclic and SCC CGR Response of a Cr-depleted 1st Layer High Cr Ni-base Weldment

The effect of the local elemental concentration is unclear. While the Alloy 52M WOL SCC CGR data (Fig. 29) appears to show a trend, the Alloy 152-LAS SCC CGR data (Fig. 27) shows a large scatter, and no clear Cr effect. The plausible reasons for the scatter are off-plane cracking as well as possible differences in the local microstructure and Cr concentration. Off-plane cracking was well-documented in these tests, hence the inability of the DC potential method to measure the SCC CGRs correctly in such cases may be partly responsible for the data scatter. However, it is important to note that relatively fast SCC in the 1st layer of Alloy 152-LAS (approx. 25 wt. % Cr) was observed in both weld directions, along and normal to the dendritic grains (Fig. 9, IG-2 and Fig. 20, IG-2). The mechanism that triggers one fracture mode over the other is not at all understood. Further complicating the analysis is the fact that microstructures having even less Cr (approx. 20 wt. % Cr, see for example the "streaks" in Fig. 19) appeared to slow down/arrest crack propagation. Moreover, the cross section shown in Fig. 25c does not suggest that SCC tends to propagate towards the interface with the LAS, or along an expected Cr gradient as one would expect if Cr content were to play a dominant role in the SCC at hand. In summary, there appears that the elemental concentration - in a simplistic interpretation, i.e., Cr content - does not seem to be a good predictor for the (local) SCC susceptibility.

Despite the lack of clear trends in the SCC CGR data or an understanding of the mechanism(s) at work, the SCC in 1st layer of Alloy 52M-182 WOL and Alloy 152-LAS (approx. 25 wt. % Cr) seem to occur in similar fracture modes (Fig. 30) and have equivalent CGRs (Figs. 27 and Fig. 29). As such there appears that the substrate – Alloy 182 or Alloy 533 LAS – plays no role. The only difference was found to occur in cases where the cracks intersected the interface with the substrate: at the Alloy 52M-182 interface, the

SCC CGR is even faster than in the 1st layer of Alloy 52M, while SCC is arrested at the intersection with the Alloy 152-LAS interface.

CONCLUSIONS

SCC CGR testing was conducted on two specimens aligned in the first layer of Alloy 152-LAS butter. The environmental enhancement was found to be a good predictor for the SCC response. Both cyclic and SCC CGR response was similar to that observed for the 1st layer of Alloy 52M-182. In both cases, in the most favorable orientations, the SCC CGRs were within a factor 2 of the MRP-115 75th percentile curve. Based on the data and analysis presented in this paper, there appears that the elemental concentration - in a simplistic interpretation, i.e., Cr content - does not seem to be a good predictor for the (local) SCC susceptibility.

ACKNOWLEDGEMENTS

The authors gratefully acknowledge the financial support from the U.S. Nuclear Regulatory Commission, job code V-6279. The views expressed in this paper are those of the authors, not necessarily those of the U.S. Nuclear Regulatory Commission.

REFERENCES

[1] Materials Reliability Program: Resistance of Alloys 690, 52 and 152 to Primary Water Stress Corrosion Cracking (MRP-237, Rev. 1): Summary of Findings From Completed and Ongoing Test Programs Since 2004. EPRI, Palo Alto, CA: 2008. 1018130.

[2] Materials Reliability Program: Resistance of Alloys 690, 152, and 52 to Primary Water Stress Corrosion Cracking (MRP-237, Rev.2): Summary of Findings Between 2008 and 2012 from Completed and Ongoing Test Programs. EPRI, Palo Alto, CA: 2013. 3002000190

[3] Materials Reliability Program: Resistance to Primary Water Stress Corrosion Cracking of Alloy 690 in Pressurized Water Reactors (MRP-258). EPRI, Palo Alto, CA: 2009. 1019086.

[4] B. Alexandreanu, Y. Chen, Ken Natesan, and W. J. Shack, Update on PWSCC Testing of Ni-base Alloys, EPRI Expert Panel, Tampa, FL, November 28-30, 2012

[5] B. Alexandreanu, Y. Chen, Ken Natesan, and W. J. Shack, Stress Corrosion Cracking of a 52M Weld Overlay in a PWR Environment, this conference.

[6] Materials Reliability Program: Crack Growth Rates for Evaluating Primary Water Stress Corrosion Cracking (PWSCC) of Alloy 82, 182, and 132 Welds (MRP-115), EPRI, Palo Alto, CA: 2004. 1006696.

[7] Alexandreanu, B., O. K. Chopra, and W. J. Shack, "Crack Growth Rates of Nickel Alloy Welds in a PWR Environment," NUREG/CR–6907, ANL–04/3, May 2006.

[8] Alexandreanu, B., O. K. Chopra, and W. J. Shack, "Crack Growth Rates of Nickel Alloys from the Davis-Besse and V. C. Summer Power Plants in a PWR Environment," NUREG/CR–6921, ANL–05/55, November 2001.

[9] Alexandreanu, B., Chopra, O.K., Shack W.J., The Stress Corrosion Cracking Behavior of Alloys 690 and 152 Weld in a PWR Environment, 2008 ASME Pressure Vessel and Piping Division Conference, Chicago, IL, July 27-31, 2008.